Widespread inhibitory projections from the interposed cerebellar nucleus

Elena N. Judd[1], Samantha M. Lewis[1], Daniel G. Heck[1], Abigail L. Person[1]

1. Department of Physiology and Biophysics, University of Colorado School of Medicine, Anschutz Medical Campus

Contact: <abigail.person@cuanschutz.edu>

Abstract

The cerebellum consists of parallel parasagittal modules that contribute to diverse behaviors, spanning motor to cognitive. Recent work illustrating a role for the anterior interposed nucleus (IntA) in reach control in mice raised questions of its anatomical organization that could confer functional specificity. We employed intersectional cell- and projection- specific labeling methods to map IntA inputs and outputs. In contrast to long-standing dogma of primarily excitatory outputs and restricted inferior olive targeting inhibitory output, we found that inhibitory IntA neurons ramified widely within the brainstem, targeting both motor- and sensory-related nuclei, suggesting potential functional roles in disinhibitory control or predictive sensory cancellation. Using monosynaptic rabies tracing, we then found that excitatory output neurons receive fewer and more precisely organized inputs than inhibitory neurons, which may set them up for distinct computations. Together these data suggest IntA contains at least two distinct output circuits and promise advances in identifying parallel computations of the cerebellum.

Introduction

The cerebellum plays a critical role in refining motor control through learning. The sole output structures of the cerebellum, the cerebellar nuclei (CbN), are proposed to relay predictive computations of the cerebellar cortex and store well-learned patterns, placing the nuclei in a central position to implement cerebellar control. The CbN house diverse neuronal subtypes that differ in their targets. Recent studies have greatly expanded our understanding of this diversity, using approaches such as genomic profiling and projection specific tracing (Bagnall et al., 2009; Chan-Palay, 1977; Fujita et al., 2020; Kebschull et al., 2020; Uusisaari & Knöpfel, 2010, 2011; Uusisaari et al., 2007; Husson et al., 2014; Ankri et al., 2015; Canto et al., 2016). Through these studies, we know that multiple diverse output channels intermingle (Fujita et al., 2020; Low et al., 2018; Sathyamurthy et al., 2020), widespread collateralization is common, and genetic diversity of excitatory projection neurons varies systematically along the medio-lateral extent of the nuclei (Kebschull et al., 2020).

The mouse anterior interposed nucleus (IntA) mediates conditioned eyelid responses as well as sculpts reach kinematics (Becker & Person, 2019; Cooper et al., 2000; Low et al., 2018; ten Brinke et al., 2017). IntA excitatory neurons project to a variety of motor related spinal cord and brainstem targets, as well as collateralize to motor thalamus. Functional studies suggest multiple cell types of the nuclei may play a role in limb control in reaching and locomotion. Ablation of a subset of IntA glutamatergic cells that express Urocortin3, for example, disrupts accurate limb positioning and timing during a reach to grasp task and locomotion (Low et al., 2018). Excitation

of presumptive glutamatergic cells demarcated by Ntsr1-cre in IntA disrupts endpoint positioning in a reach to grasp task (Becker & Person, 2019). Finally, chemogenetic silencing of excitatory neurons that project ipsilaterally to the spinal cord also interfered with reach success in mice (Sathyamurthy et al., 2020). Together, these studies suggest projections from diverse types within IntA to forelimb movement related brain structures may provide a substrate for the CbN to coordinate movement precision and balance during forelimb tasks.

Understandably, these studies have focused almost exclusively on glutamatergic cell types. Interestingly, however, ablation of nucleo-olivary cells demarcated with Sox14 expression also resulted in motor coordination deficits, while not impairing associative learning (Prekop et al., 2018). This motor deficit is surprising since inhibitory output neurons from intermediate and lateral nuclei are expected to only innervate the IO. The medial nucleus (fastigial) is thought to be unique among the nuclei in that its inhibitory output population includes large glycinergic neurons that project to ipsilateral brainstem targets outside the IO (Bagnall et al., 2009). Indeed, consistent with traditional views of GABAergic output channels, tracing of Sox14-Cre neurons of the lateral nucleus revealed projections to the IO (Prekop et al., 2018). However, hints in the literature suggest that there may be more extensive inhibitory output from the nuclei than is currently appreciated (Locke et al., 2018; Turecek & Regehr, 2020). Nevertheless, inhibitory projections from intermediate cerebellum have not been the focus of investigation, to our knowledge.

Here we use a range of viral tracing methods to isolate and map projections from and to different IntA cell types, including inhibitory neurons, defined through intersectional labeling methods using single or multiple recombinases coupled with pathway-specific labeling (Fenno et al., 2014). This method permitted analysis of collateralization more powerful than traditional dual-retrograde labeling strategies. We elucidate the projection “fingerprints” of specific cell-types and projection-types. Surprisingly, we observed widespread inhibitory outputs, comprised of putative collaterals of IO-projecting neurons, that target both ipsilateral and contralateral brainstem and midbrain structures, with implications for a novel role of inhibitory neurons in online motor control and regulating IO error signaling. Monosynaptic rabies transsynaptic tracing (Kim et al., 2016; Wickersham et al., 2010) restricted to excitatory premotor neuron populations through the selective expression of Cre recombinase under the Ntsr1promoter (Gong et al., 2007) and inhibitory neurons through Cre expression controlled under the Gad1 locus (Higo et al., 2009; Vong et al., 2011) revealed dramatically distinct and reproducible patterns of presynaptic inputs labeled following rabies expression targeted to distinct cell classes in the nuclei. Together these experiments provide new insight into input/output diversity of the intermediate cerebellum, suggest potential functional diversity of parallel channels, and provide anatomical targets for functional studies aimed at evaluating these putative roles.

Results

Anterograde tracing of inhibitory IntA neurons

To determine projection patterns of inhibitory neurons of IntA (iIntA), we selectively labeled them in Gad1-Cre (n = 5) or Vgat-Cre (n = 4, See Methods) transgenic mice injected with AAV2.EF1a.DIO.YFP. Based on previous literature suggesting that inhibitory projections to targets other than IO may be restricted to large glycinergic neurons which are absent from IntA (Ankri et al., 2015; Bagnall et al., 2009; Esposito et al., 2014; Prekop et al., 2018), we expected

projections from iIntA to exclusively target IO. However, in both transgenic lines, axon terminals were labeled throughout the brainstem and midbrain, suggesting previously unknown projections of inhibitory neurons from IntA.

As expected, iIntA neurons densely innervated the dorsal accessory olive (Figure 1C). Moderate label in the principle subnucleus and Cap of Kooy, a known target of VEST suggested some potential for injection site spillover (but see below; (Balaban & Beryozkin, 1994; Fredette & Mugnaini, 1991; Prekop et al., 2018; Ruigrok & Voogd, 1990, 2000; Want et al., 1989). Inhibitory IntA neurons also produced extensive terminal fields outside IO, within the medulla and midbrain. Modestly dense but spatially extensive terminal fields ramified in the posterior medulla along the anterior-posterior axis, with ipsilateral label in the dorsal medullary reticular nucleus (MDRNd), parvicellular reticular nucleus (PARN) and bilateral label in the gigantocellular reticular nucleus (GRN) and the ventral region of the medullary reticular nucleus (MDRNv) indicating connectivity with forelimb associated brainstem nuclei (Esposito et al., 2014) (Figure 1C). We did not observe iIntA terminals or axons within the spinal cord of any specimens, suggesting that iIntA neurons do not directly influence circuits within the spinal cord.

iIntA axons extended through the pontine reticular nuclei (PRN) to innervate the tegmental reticular nucleus of the pons (TRN) and the basilar pontine nuclei (Figure 1D), common precerebellar mossy fiber centers. iIntA neurons also innervated medial RN (Figure 1E) with unique morphology, as if terminals focally innervated individual or small clusters of RN somata, a morphological trait not observed following labeling of excitatory neurons (see Figure 5A). Vgat neurons targeted RN bilaterally while Gad1 neurons only innervated the contralateral RN. iIntA axons progressed to the caudal diencephalon, targeting the ipsilateral ZI (2/4 Vgat and 1/5 Gad1 specimen) and the contralateral thalamus (VM, VPM, VAL) in a similar location as observed for excitatory neurons (see below). However, Vgat neurons did not target VAL or VM. Among sensory brainstem structures, terminal fields ramified within subdivisions of the ipsilateral external cuneate nucleus (ECU), dorsal column nuclei (DCN), nucleus of the solitary tract (NTS), spinal trigeminal nucleus (SPV), especially the lateral edge, parabrachial nuclei (PB), and principle sensory nuclei of the trigeminal (PSV). Vgat neurons generally targeted these regions more strongly than Gad1 neurons, though terminals were identified in both transgenic lines.

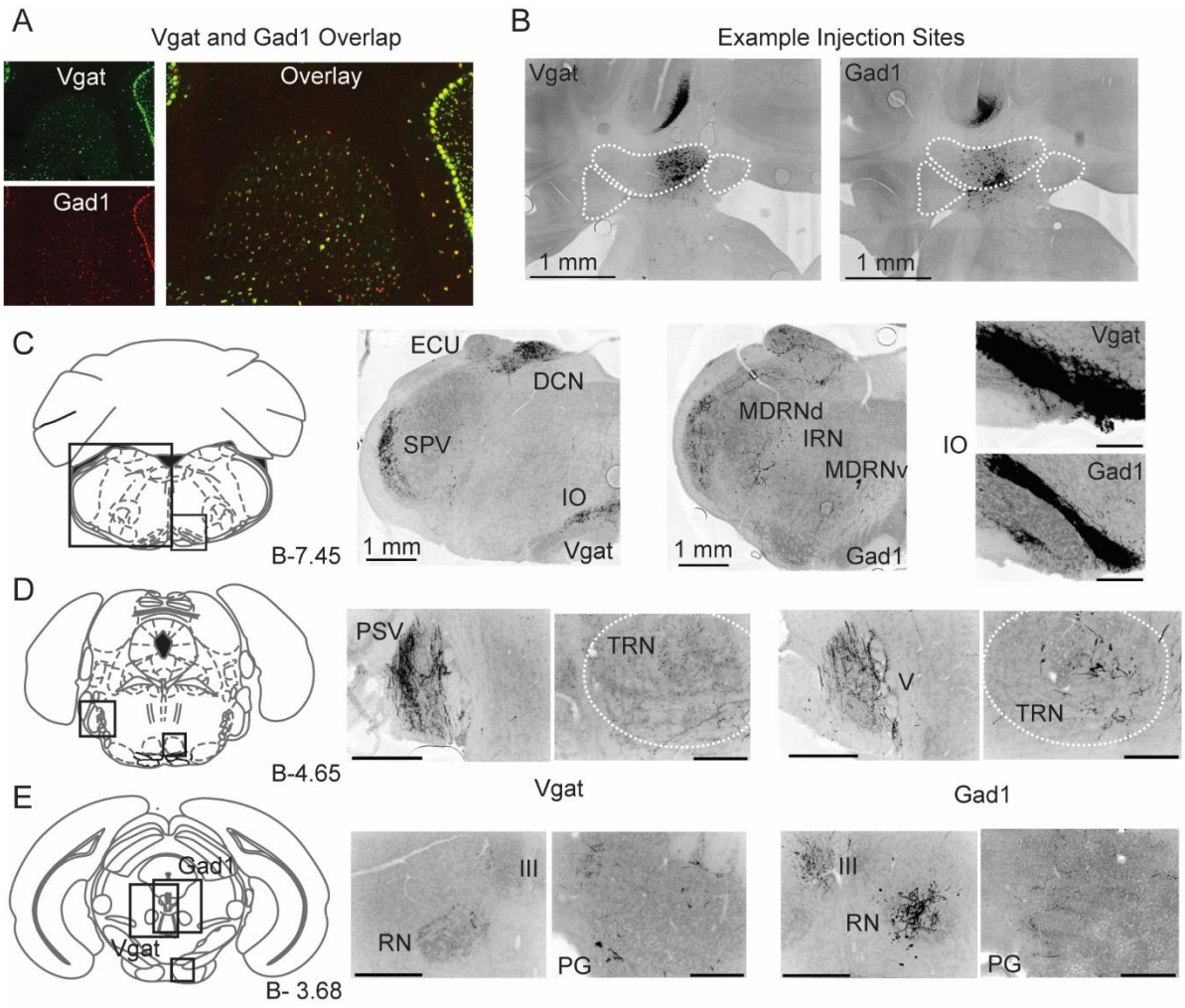

Figure 1. Inhibitory projections from IntA. (A) Dual fluorescent in situ hybridization showing largely overlapping populations of Vgat+ and Gad1+ cells within Int. Purkinje cells seen to right of image expressing both Gad1 and Vgat. (B) Example injection sites within Gad1-Cre and Vgat-Cre mice. Boundaries of the cerebellar nuclei are outlined. Scale bars represent 1 mm. Images are oriented so that ipsilateral projections are depicted left and contralateral projections are depicted as right of midline in Atlas images. Dense label ventral to IntA are exiting axons. (C) Example terminal fields in the ipsilateral caudal brainstem (approximately 7.45 mm posterior to Bregma). Terminals from example Vgat-Cre mouse (left) and Gad1-Cre mouse (right). Scale bar = 1 mm. Terminals within the IO (far right) in Vgat-Cre (top) and Gad1-Cre (bottom) mice. Scale bar = 200 µms. ECU = external cuneate nucleus, DCN = dorsal column nuclei, SPV = spinal trigeminal nucleus, IO= inferior olive, MDRN = medullary reticular nucleus (dorsal, d, or ventral, v), IRN = intermediate reticular nucleus. (D) Example terminal fields in the rostral brainstem (approximately 4.65 mm posterior to Bregma). Dense innervation of the PSV (principle sensory nucleus of the trigeminal, left, scale = 500 µms) and sparse innervation of the TRN (tegmental reticular nucleus of the pons, outlined, right, scale = 200 µms) in Vgat-Cre (left group) and Gad1-Cre mice (right group). Note terminal fields in TRN are denser in Gad1 than Vgat-Cre mice. (E) Example terminal fields in the midbrain (approximately 3.68 mm posterior to Bregma). Sparse targeting of the ipsilateral RN (red nucleus) and III (oculomotor nucleus, left-most image, scale bar = 500 µms) and anterior contralateral PG (pontine grey, scale bar = 200 µms) in example Vgat-Cre mouse shown in left group. Denser targeting of the ipsilateral III and contralateral RN (scale bar = 500 µms) but more sparse targeting of the anterior contralateral PG (scale bar = 200 µms) seen in Gad1-Cre example mouse. The rostral PG (B-3.93) is more heavily targeted than the anterior PG (shown here); see Figures S1 and S2 for example terminals in this region.

As expected, we observed innervation of the cerebellar cortex by iIntA in all 9 animals, especially to lobules 8-9, Cop, and the flocculus (Fl), terminating in the granule cell layer of the cerebellar cortex with beaded axons (see Figure 5A for example (Ankri et al., 2015)). Vgat neurons targeted all cerebellar lobules, even extending contralaterally to target lobules in

the opposite hemisphere (see Table 1 for a full list of brain regions targeted and average projection strengths). We observed a less consistent projection to lobules 4 /5, Cr 1/ 2, PM, and Simplex (1-3 of 6 specimens) by Gad1-Cre mice. Several specimens showed minor label of inhibitory cells in the ventral Cb-Ctx just dorsal to IntA, but nucleocortical terminals that were included in the projection analysis were not located in the same topographical area.

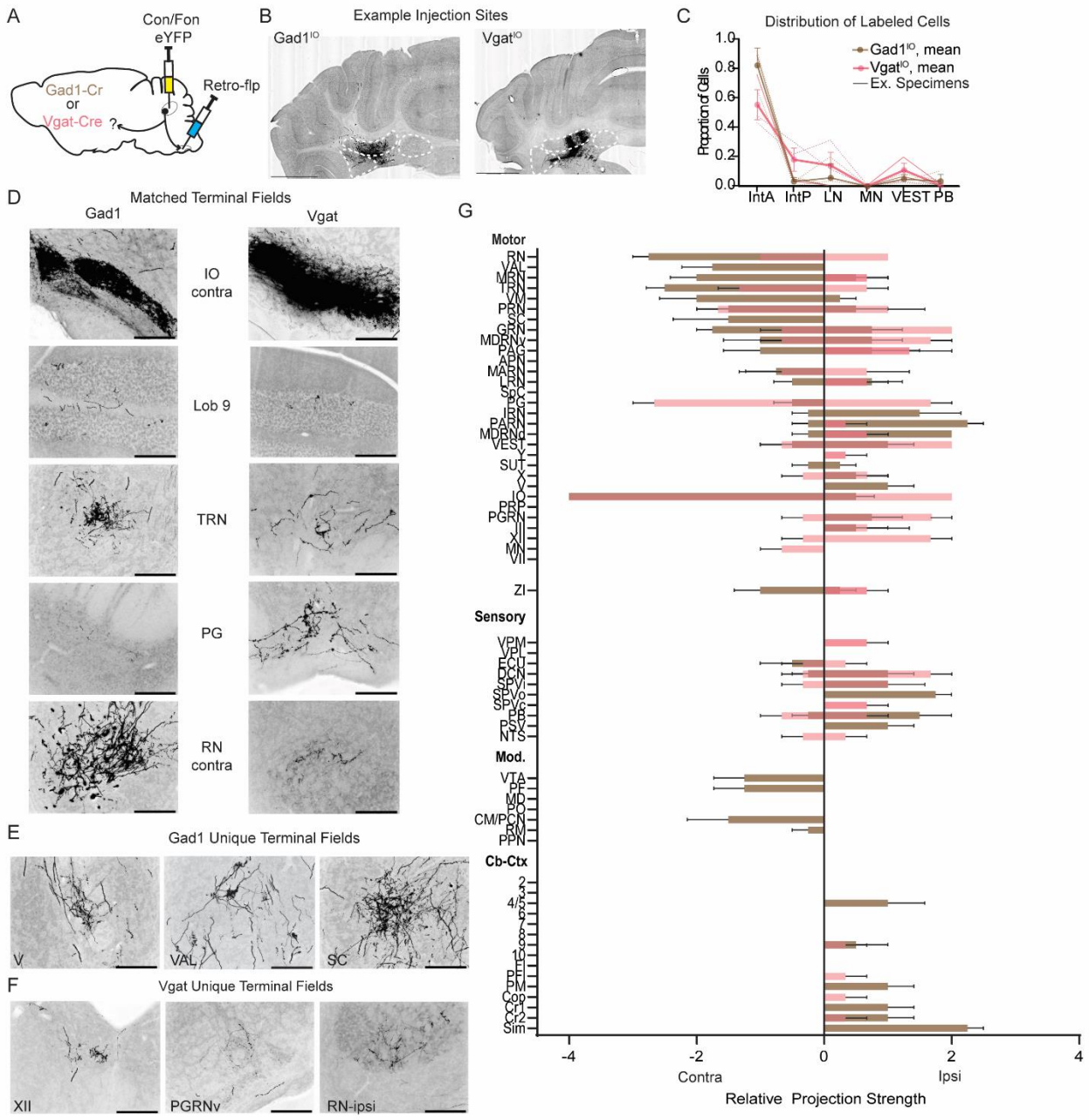

Figure 2. Intersectional labeling of IO-projecting inhibitory neurons in IntA. (A) Schematic of injection paradigm. (B) Example injection sites in Gad1 (left) or Vgat (right)-Cre mice. Scale bar represents 1 mm. (C) Analysis of the distribution of labeled cells from initial injection of Con/Fon-eYFP. Pink denotes Vgat-Cre specimens, brown denotes Gad1-Cre specimens. Data with symbols are the mean for all specimen within the cohort, individual specimen data are shown with dotted lines, and the example specimen whose terminal fields are imaged below are depicted with a solid line. (D) Matched terminal fields within IO (inferior olive), Lob9, TRN (tegmental reticular nucleus of the pons), PG (pontine grey), and RN (red nucleus) are seen in both Gad1 (left) and Vgat-Cre (right) mice. Scale bars = 200 µms. Note Vgat-Cre neurons project more densely to PG and less densely to TRN and RN than Gad1-Cre neurons. (E) Terminal fields unique to Gad1-Cre mice: V (facial motor nucleus, left),

VAL (ventral anterior lateral nucleus of the thalamus, middle), SC (superior colliculus, right). Scale bars = 200 µms. (F) Terminal fields unique to Vgat-Cre mice: XII (hypoglossal nuclei, left), PGRN (paragigantocellular reticular nucleus, ventral; middle), ipsilateral RN (right). Scale bars = 200 µms. (G) Graphical representation of average projection strength in all targeted regions for Gad1^{IO} (n = 4; brown) and Vgat^{IO} (n = 3; pink) mice.

Intersectional label of iIntA projections to IO

The terminal labeling observed in brainstem and midbrain following Gad1 and Vgat-Cre restricted label of iIntA strongly suggested widespread inhibitory channels from the intermediate cerebellum. Several important questions and caveats remained, however, including that Purkinje neuron label was unavoidable with direct injection into Gad1-Cre and Vgat-Cre IntA. We next used an intersectional approach to restrict label to IO-projecting iIntA neurons (Fenno et al., 2017). In Gad1-cre (n=4) and Vgat-cre mice (n=3), we injected the contralateral IO with AAVretro-EF1a-Flp followed by a two-recombinase-dependent reporter virus (AAV8-hsyn-ConFon-eYFP) into IntA (Figure 2A-B). This method isolated IntA neurons which project to IO and were Gad1 or Vgat positive. Injections in wildtype C57/Bl6 mice (n=2) and off-target injections in Gad1-Cre mice (n=3) did not yield YFP positive neurons in the nuclei. Thus, this method both identifies putative collaterals of IO-projecting iIntA neurons and controls for the possibility of non-IO projecting non-specific Cre expression in IntA accounting for brainstem label.

Similar to direct injections into iIntA neurons, IO-projecting iIntA innervated forelimb control associated regions RN, GRN, MDRNv and PARN (Figure 2D, G), even in the most finely targeted injections. Both cohorts produced terminals in the TRN and PG, though Gad1^{IO} showed a preference for TRN and Vgat^{IO} produced denser terminals in PG (Figure 2D). We consistently observe terminals in sensory regions SPV, DCN, ECU, and PB with intersectional label of both Vgat^{IO} and Gad1^{IO}. Nucleocortical terminals were observed using intersectional approaches in both transgenic lines, especially in Crus2 and lobule 9 (Figure 2D, G). In contrast, Gad1^{IO} (n = 4) targeted intermediate cerebellar lobules such as 4/5 and Sim while Vgat^{IO} (n = 3) targeted Cop and PFl. Gad1^{IO} and Vgat ^{IO} neurons labeled terminals in numerous brainstem and midbrain areas, largely corroborating the core results from direct iIntA labeling methods (Figure 1).

Despite the consistency of most targets across labeling methods, some regions were targeted by only one transgenic line. Gad^{IO} neurons innervated MDRNv, IRN, V, PSV, SC, and thalamic nuclei, VAL, CM/PCN, PF, and VM (Figure 2E, G). Vgat^{IO} neurons produced terminal fields in the ventral PGRN (PGRNv), XII, ipsilateral ZI, and VPM that were not seen in Gad1^{IO} injections (Figure 2F, G). Additionally, Vgat^{IO} produced sparser bilateral terminals in RN corroborating the results of projection non-specific tracing. A table summarizing termination patterns of iIntA neurons following these four labeling methods indicates that brainstem and midbrain targets are consistently innervated by these cells while diencephalic projections were only observed in Gad1-cre mice (Table 1).

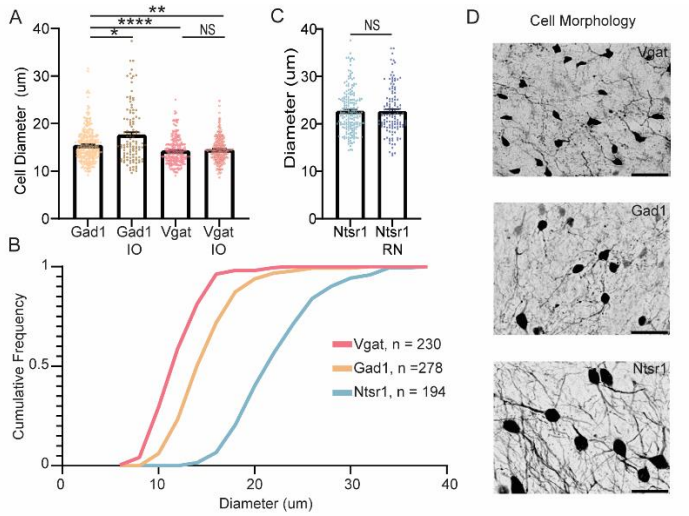

Figure 3. Cell sizes differ across classes. (A) Differences in soma diameter of inhibitory IntA neurons based on isolation method. Mean ± SEM is plotted. Gad1 neurons (n = 278, 5 mice) are smaller than Gad1^{IO} (n= 113, 4 mice) neurons (p= 0.01; Mann-Whitney unpaired, two tailed T-test) and larger than Vgat (n = 230, 3 mice; p<0.0001; Mann-Whitney unpaired, two tailed T-test) or Vgat^{IO} neurons (n = 245, 3 mice; p = 0.009; Mann-Whitney unpaired, two tailed T-test). (B) Cumulative frequency distribution of measured cell diameter for Vgat, Gad1, and Ntsr1-Cre specimens (n = 194, 5 mice). (C). Ntsr1 and Ntsr1^{RN} (n = 125, 4 mice) label neurons of the same size (p = 0.8; Mann-Whitney unpaired, two tailed T-test). Mean ± SEM is plotted. (D) Example YFP+ cells in a Gad1 (top), Vgat (middle) and Ntsr1 (bottom) specimen. Scale bars represent 50 µms. P<0.05, *, p<0.01, **, p<0.001, ***, p<0.0001, ****.

IntA cell sizes differ according to Cre and intersectional drivers

To better characterize the neurons labeled with these distinct targeting methods, we measured the cross-sectional area and elliptical diameter of soma across targeting methods. We found Gad1^{IO} neurons (17.7 ± 0.6 µm diameter; 165.7 ± 9.9 µm^2 area, mean ± SEM, n = 113, 4 mice) to be slightly larger than the superset of Gad1 neurons (15.5 ± 0.2 µm diameter, p = 0.01, 135.7 ± 4.3 µm^2 area, p = 0.06; mean ± SEM; Figure 3). Local interneurons are thought to be smaller than GABAergic projection neurons, so this size difference could be attributable to the lack of interneuron label (Batini et al., 1992; Chan-Palay, 1977; De Zeeuw & Berrebi, 1995; Fredette & Mugnaini, 1991; Schwarz & Schmitz, 1997; Teune et al., 1998; Uusisaari et al., 2007). In contrast, Vgat-Cre (14.3 ± 0.2 µm diameter, 107.3 ± 2.5 µm^2 area) and Vgat^{IO} labeled neurons of similar sizes (14.6 ± 0.2 µm diameter, p = 0.08; 103.1 ± 1.8 µm^2 area, p=0.83; mean ± SEM, n = 245, 3 mice; Figure 3A).

Finally, we compared these populations to putative excitatory neuron cell sizes. First, we validated Ntsr1-Cre (gn220) as a cerebellar nuclear cre driver line labeling non-GABAergic neurons (Dumas et al., 2019). Examination of publicly available dual fluorescent in situ hybridization expression showed non-overlap of Ntsr1-Cre expression with Gad1 (Figure S1A). We quantified colocalization of Ntsr1 and Gad1 signal by analyzing pixel overlap relative to Vgat, Gad1, and Vglut2 colocalization as controls (Figure S1B). Gad1 and Ntsr1 overlap (average of 19%) was within the noise of presumptive non-overlapping markers, Vglut2 and Vgat (average of 17% overlap). In contrast, Gad1 and Vgat had largely overlapping (average of 83%) fluorescent pixels in both channels. These data support the conclusion that Ntsr1-Cre and Gad1-Cre label largely non-overlapping IntA populations (See methods; (Higo et al., 2009; Houck & Person, 2015)).

The cells labeled by injection into Ntsr1-cre transgenic animals were characteristically large multipolar cells (22.7 ± 0.3 µm diameter; 237.6 ± 5.2 µm^2 area, mean ± SEM; Figure 3B). On average, Gad1 cells were smaller than those labeled in Ntsr1-Cre mice ($p < 0.0001$), though a substantial subset were approximately equal sized (Bagnall et al., 2009; Batini et al., 1992; Canto et al., 2016; Prekop et al., 2018; Ruigrok & Teune, 2014; Uusisaari et al., 2007). The smaller cells possessed shorter, spikey dendrites with tortured paths, compared to the long, smooth dendrites of large neurons. Vgat neurons tended to be composed of the smaller, more fibrous neurons (12.7 ± 0.2 µm diameter, 70.5 ± 1.4 µm^2 area; $p<0.0001$; mean ± SEM; Figure 3D). When we isolated RN-projecting Ntsr1 neurons using the multiple recombinase method as previously described, we did not find a difference in cell size (22.7 ± 0.4 µm diameter; 241.2 ± 6.8 µm^2 area, mean ± SEM; Figure 3C). Together, these results substantiate the argument that iIntA injections using various methods label distinct cell populations that innervate previously unknown targets in the brainstem.

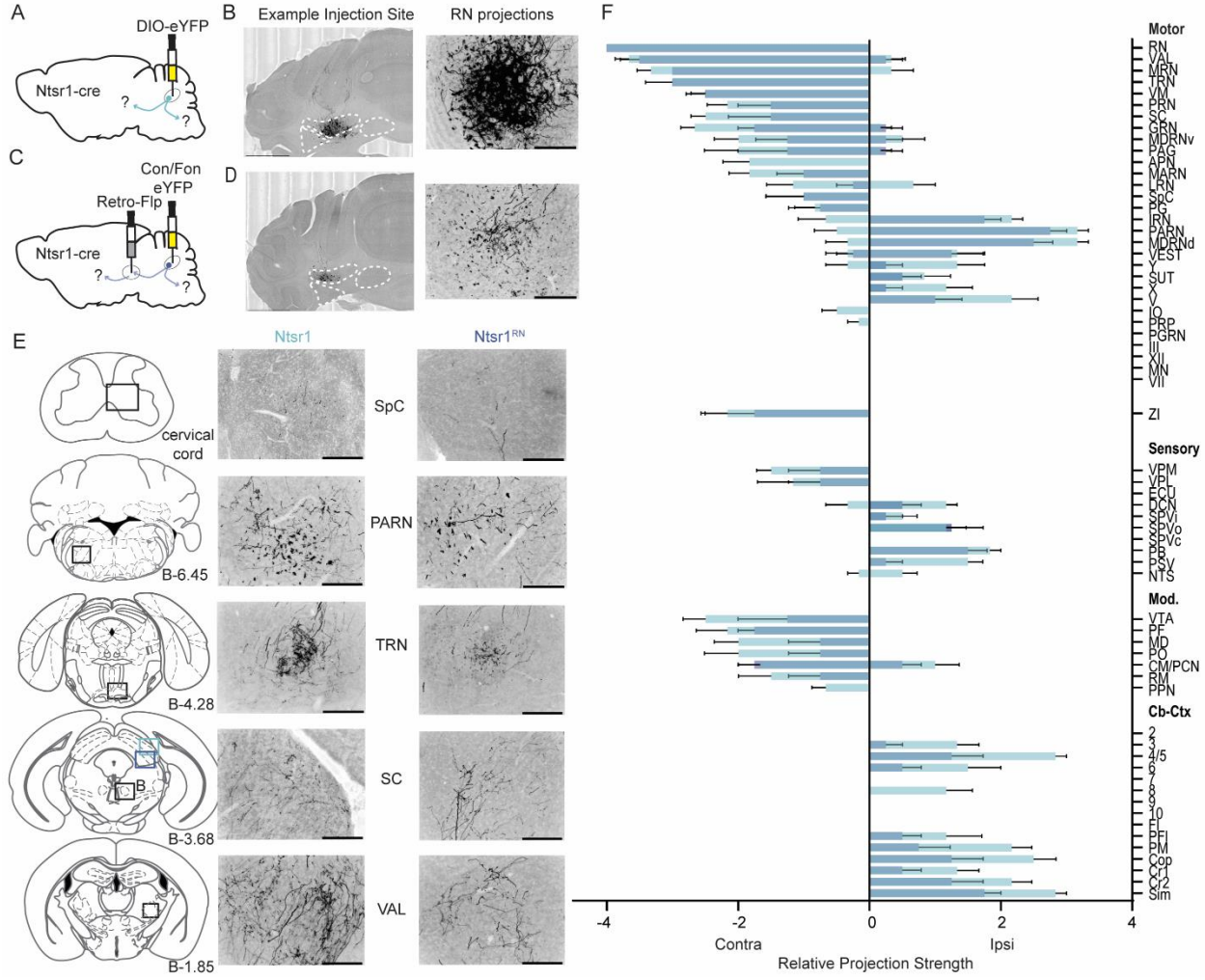

Figure 4. Ntsr1 and Ntsr1^{RN} label a homogenous cell population that collateralizes to many brain regions. (A) Schematic of injection paradigm labeling Ntsr1 positive neurons in IntA. (B) Example injection site (left; scale bar = 1 mm) and terminals in RN (right; scale bar = 200 µms). (C) Schematic of injection paradigm labeling RN-projecting Ntsr1 neurons in IntA. (D) Example injection site (left; scale bar = 1 mm) and terminals in RN (right; scale bar = 200 µms). Note small injection site and relatively sparser innervation of RN influences the projection strength assignments in other regions. (E) Terminal fields observed in SpC (cervical spinal cord, top), PARN (parvicellular reticular nucleus), TRN (tegmental reticular nucleus), SC (superior

colliculus), and VAL (ventral anterior lateral nucleus of the thalamus, bottom) using projection non-specific (left column) and projection specific (right column) labeling of Ntsr1 neurons. Scale bars = 200 µms. (F) Graphical representation of average projection strength in all targeted regions for Ntsr1 and Ntsr1^{RN}. Note large degree of overlap. A list of abbreviations can be found below.

Anterograde tracing from excitatory output neurons

At first glance, the projections from iIntA neurons appear to recapitulate targets of the putative excitatory population. To compare iIntA projections more directly to excitatory outputs, we injected IntA of Ntsr1-Cre mice with AAV1.CAG.flex.GFP (n =3) or AAV2.DIO.EF1a.eYFP (n=2) (Figure 4A-D). As expected, tracing Ntsr1-Cre neurons from IntA (nIntA) revealed widespread fluorescent terminal fields in the ipsilateral and contralateral caudal brainstem, the contralateral rostral brainstem, the contralateral thalamus (Houck & Person, 2015; Low et al., 2018), and layers 7/ 8 in the contralateral cervical spinal cord of 2/ 4 available spinal cords (Figure 4E; (Sathyamurthy et al., 2020)). nIntA neurons formed nucleocortical mossy fibers in posterior lobules, such as Paramedian (PM), Copula (Cop), Crus 1/ 2 (Cr1, Cr2), as well as more anterior intermediate lobules such as 4/5 and Simplex (Sim) (Gao et al., 2016; Houck & Person, 2015; Tolbert et al., 1978).

nIntA neurons produced reliable boutonal label in forelimb medullary structures such as the MDRNv, PARN, GRN, pontine reticular nuclei (PRN) and magnocellular reticular nucleus (MARN; Figure 4E; (Esposito et al., 2014)). nIntA also labeled terminals in the GRN/ MARN region resided just dorsal to the boundary of IO (See supplement). Additionally, in 3 of 6 animals, we observed a small patch of terminals within the dorsal subnucleus of IO (Figures 5A, S4). We currently are unable to determine if this label was a consequence of promiscuous Cre expression or if a group of Ntsr1 defined glutamatergic or GABAergic neurons project to IO. Exclusive retrograde labeling of IO-projecting Ntsr1 neurons was not practical, due to the proximity of nIntA terminals just dorsal to IO, in the ventral brainstem.

nIntA projected to many motor-related regions including the lateral reticular nucleus (LRN); all four subdivisions of the vestibular nuclei (VEST), and the motor nucleus of the trigeminal (V). Axons extended contralaterally through the PRN, ultimately producing dense innervation of the TRN (Figure 4E) and limited innervation of the PG (Cicirata et al. 2005; Schwartz and Schmitz 1997). nIntA axons innervated the contralateral RN most densely, with terminals spilling over into the ventral tegmental area, VTA (Figure S4) (Carta et al., 2019) and extended upward through the contralateral MRN to innervate the caudal anterior pretectal nucleus (APN; (Sugimoto et al., 1982)) anterior ventrolateral periaqueductal grey (PAG; B- 4.0-2.4 mm), and intermediate/ deep layers of the SC (Doykos et al., 2020; Gayer & Faull, 1988), especially the more rostral and lateral regions (B-3.8-2.8 mm; Figure 4E). Consistent projections were also observed in brainstem sensory structures targeted by iIntA including: SPV, DCN, PB (especially the Koelliker-Fuse (KF) subnucleus), and PSV. In addition to VTA, other modulatory regions, such as the raphe magnus nucleus (RM) and pedunculopontine nuclei (PPN) were targeted by nIntA.

At the level of the diencephalon, projections were consistently observed within the contralateral Zona Incerta (ZI) and thalamus (Figure 4E-F). All specimens exhibited dense terminal fields in the ventromedial (VM) and anterior ventrolateral (VAL) nuclei of the thalamus (Aumann et al., 1994; Houck & Person, 2015; Kalil, 1981; Low et al., 2018; Stanton, 1980). Additionally, we observed terminals in intralaminar thalamic structures including: centromedial (CM), paracentral

(PCN), mediodorsal (MD) parafascicular (PF), ventral posterior (VP), and posterior (PO) nuclei(Chen et al., 2014; Dumas et al., 2019).

A dominant theme in IntA output projections is collateralization. Recent studies have identified other Cre driver lines (Low et al., 2018) labeling subsets of IntA output neurons, raising the question whether Ntsr1-Cre projection patterns reflect multiple subsets of neurons or broadly reflect a relatively homogenous population that collateralizes widely. To begin to address this question, we asked whether projection-specific labeling of nIntA recapitulated tracing from Ntsr1-Cre cells. We used the intersectional approach described above to restrict tracing to RN-projecting Ntsr1-Cre neurons (Ntsr1^{RN} Figure 4A.)

Interestingly, the projection pattern of Ntsr1^{RN} was almost identical to the pattern observed in nIntA injections, with a few notable exceptions. Namely, nIntA neurons projected to lobule 8, APN, and PPN while Ntsr1^{RN} neurons did not. We otherwise observed very similar projection patterns, including nucleocortical projections mainly targeting lobules 4/ 5, Cr2, Cop and Sim, though we observed a decreased tendency for these RN projecting neurons to target the PM lobule. We observed terminals in the contralateral thalamus, especially VAL, VM, and CM/ PCN as well as layers 7/8 of the contralateral cervical spinal cord in 2 of 3 specimens supporting the observation in Sathyamurthy et al. (2020) that contralaterally projecting cerebellospinal neurons collateralize to both RN and thalamus. We conclude it is likely that Ntsr1.cre driver lines label a population of IntA neurons which are relatively homogenous and distribute information broadly.

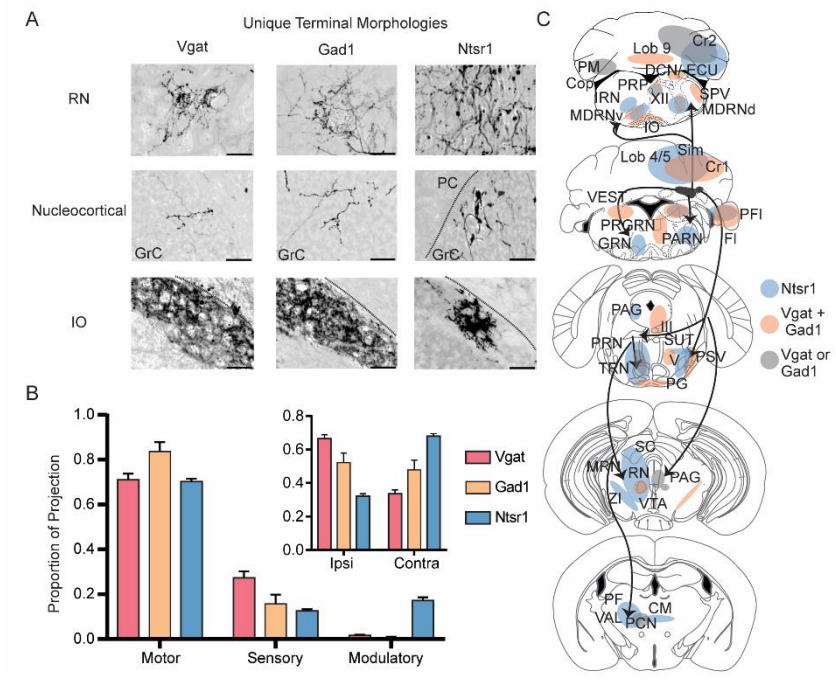

Figure 5. Comparison of iIntA and nIntA projection patterns. (A) Morphology differences in terminal contacts within RN (top), the Cerebellar cortex (middle; boutons observed within the granule cell (GrC) layer; dotted line in Nstr1 image denotes Purkinje Cell layer), and IO (bottom; dotted line indicates dorsal edge of IO). Note mossy fiber nucleocortical terminals seen in Ntrs1-Cre mice but not Gad1 or Vgat-Cre mice. (B) Analysis of average RPS contributions by motor, sensory, or modulatory extracerebellar brain regions. Inlay shows contribution of ipsilateral or contralateral projections to total RPS. (C) Schematic of projection signatures from Ntsr1-Cre (blue), Gad1 and Vgat-Cre (orange), and Gad1 or Vgat-Cre (grey). See list of Abbreviations.

Direct comparison of nIntA and iIntA projection patterns

Despite targeting many of the same brain regions, terminal morphology or projection patterns of the three transgenic lines were distinct, particularly when viewed in light of the functional role of target regions (Figure 5A). We grouped extracerebellar target regions into three functional classes -- motor, sensory, and modulatory -- based in part on groupings of the Allen Brain Atlas (see methods). Inhibitory neurons, particularly Vgat-cre neurons, targeted more sensory

structures than nIntA neurons. By contrast, nIntA specimens projected more heavily to modulatory regions than either of the inhibitory cell labeling transgenic lines and also provide direct input to the cervical spinal cord (Figure 5B).

Other relationships among the projection classes were notable (Figure 5C). Axons originating from nIntA tended to ramify in contralateral motor-related regions such as MDRNv, GRN, PRN, PAG and MRN (and mixed regions like ZI) while iIntA axons predominantly targeted these nuclei ipsilateral to the injection site. On the other hand, excitatory and inhibitory cell types produced terminals in topographically indistinguishable locations in the MDRNd, PARN, IRN, X, Y, TRN, RN, and thalamic nuclei, VAL, VM, VPM, CM/PCN. However, iIntA formed smaller terminal fields on average than did nIntA and did not project to other nIntA targets within the thalamus. iIntA projections to SC were largely absent.

Axon terminations within cranial nuclei were also largely distinct. nIntA projected more to the trigeminal motor nucleus (V), ramifying near the outer boundary. Both Vgat and Gad1 neurons projected to the oculomotor nucleus (III), however, only Vgat specimens showed terminals in the hypoglossal cranial nuclei (XII). Distinct terminal fields were identified within sensory nuclei. Inhibitory neurons labeled by both Vgat-Cre and Gad1-Cre mice projected to more lateral aspects of sensory nuclei SPV and PSV, though Vgat-Cre mice targeted a larger area of SPV including the most caudal subdivision (SPVc). Vgat-Cre mice also projected more heavily to the anterior aspect of PSV than either Gad1 or Ntsr1-cre specimens. Ntsr1-cre mice projected to the medial edge of SPV near the border with MDRNd/ PARN and to PSV near the border of V.

iIntA and nIntA projected to VEST, however, iIntA projected more to the caudal (B-7.0-6.3) spinal and medial VEST than nIntA. Both nIntA and iIntA formed nucleocortical fibers, though nIntA tended to target more intermediate lobules while iIntA cells more heavily targeted posteromedial lobules, especially lobule 9, and flocculus (Fl).

Projections of IntA^{RN} neurons traced with AAVretro-Cre

As a final control to challenge the finding that IntA neurons collateralize to both RN and IO, we injected modified AAV-retrograde-Cre virus into RN while simultaneously injecting a flexed reporter virus (AAV1- CAG-flex-GFP/ RFP) into IntA of wild type mice (C57BL/6, Charles River). This method avoids the potential pitfall of ectopic Cre expression in diverse cell types owing to developmental or other unknown causes. However, in keeping with our core observations, following these injections, we observed dense contralateral label in both IO and RN (see Table 1 for total projection profile). We also observed terminals in other locations consistently targeted by nIntA (MRN, VAL, VPM, VM, PF, MD, PO, SC, ZI) and iIntA (Lob 9, IO, SPV (lateral edge), ipsilateral PRN, and ECU). We conclude that retrograde uptake of Cre from synaptic terminals in RN results in reporter expression of both glutamatergic and GABAergic neurons in IntA, confirming the presence of a collateral projection from iIntA to both IO and RN.

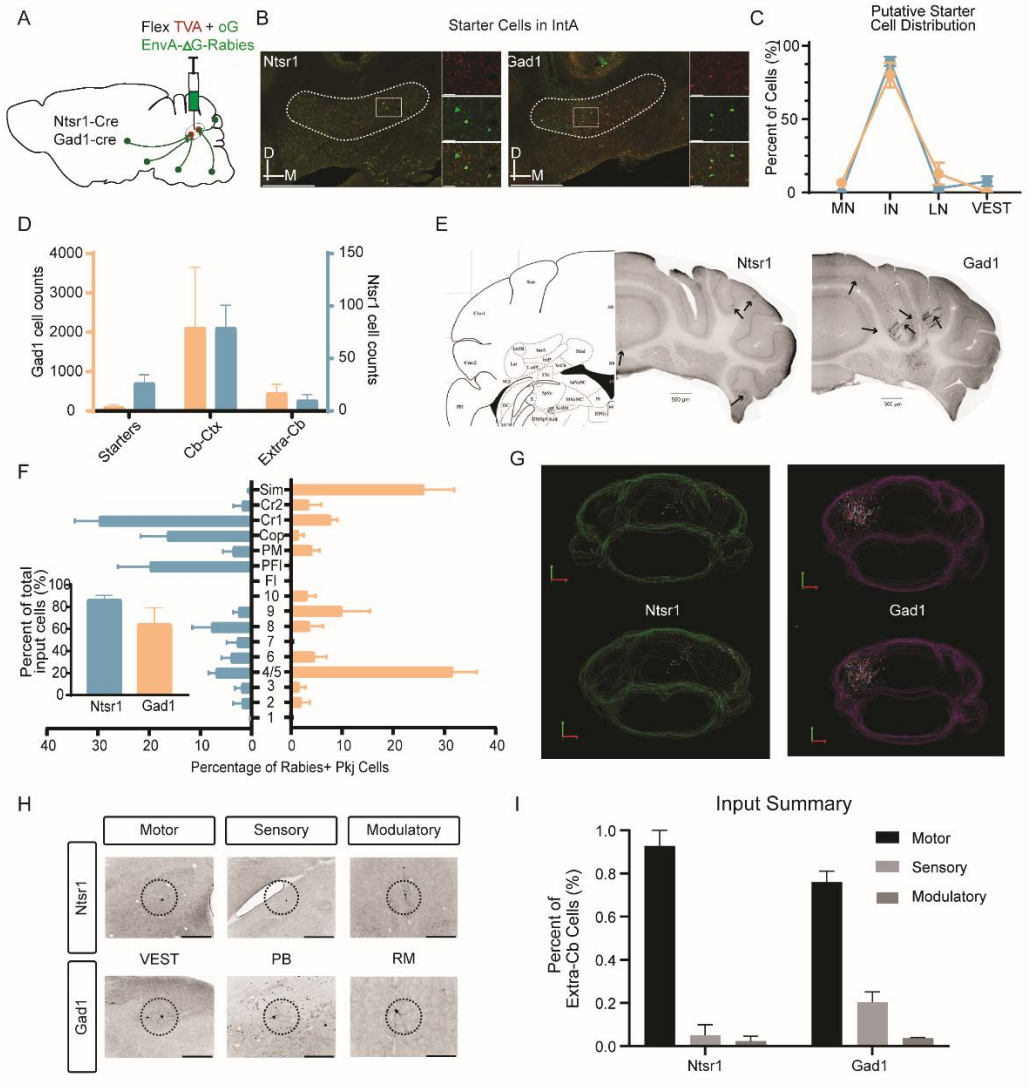

Figure 6. Monosynpatic tracing of inputs to IntA. (A) Schematic of viral tracing protocol. Cells labeled by this method provide monosynaptic input to IntA. (B) Example starter cells from both transgenic mouse lines in IntA. Scale bar = 500 µms. Insets to the right show oG/ Rabies positive cells (green channel, middle) amid TVA expression (red channel, top), and overlay (bottom). Scale bar = 50 µms. (C) Distribution of putative starter cells largely overlaps for both cell types (mean + SEM). (D) Comparison of number of cells labeled as starter neurons, retrogradely labeled Purkinje Cells (Cb-Ctx), and retrogradely labeled neurons outside of the cerebellum (ExtraCb). Gad1 numbers are plotted on the left y-axis (salmon), Ntsr1 numbers are plotted on the right y-axis (cyan). (E) Example retrogradely labeled rabies positive PCs. Scale bar = 1 mm. (F) Distribution of rabies labeled PCs in different lobules. Inlay shows percentage of all rabies positive cells (excluding starter cells) that were identified within the cerebellar cortex. (G) 3D reconstruction of retrogradely labeled PCs in each transgenic mouse line. Note restricted distribution in Ntsr1 but not Gad1 mice. (H) Example extracerebellar rabies positive cells in motor (vestibular- VEST), sensory (parabrachial- PB), and modulatory (raphe magnus- RM) brain regions for both mouse lines. (I) Percent of extracerebellar inputs to Gad1 or Ntsr1 cells separated by modality.

Cell type specific input tracing using monosynaptic rabies virus

Having mapped novel inhibitory pathways from the interposed nucleus, we next asked about afferents to diverse cell types. To identify inputs to different IntA cell types, we used modified rabies (EnvA-ΔG-Rabies-GFP) and Cre-dependent receptor and transcomplementation helper viruses (AAV1-EF1.Flex.TVA.mCherry, AAV9.Flex.H2B.GFP.2A.oG, Figure 6A, (E. J. Kim et al., 2016; Wall et al., 2010; Watabe-Uchida et al., 2012; Wickersham et al., 2007, 2010). Gad1-

cre (n = 3) and Ntsr1-Cre (n = 6) mice were used to isolate inputs to distinct IN populations (Figure 6 B). Direct rabies virus infection is limited to cells which express the necessary receptor, TVA, and the transsynaptic movement of the modified rabies virus is restricted to a single jump by the complementation of oG expression in defined cell types. In this way, we were able to identify monosynaptic inputs to a specified set of starter cells. Analyzed specimens had 86.3± 3.5% (mean ± sem; Figure 6 B-C) starter cells within Int; however Gad1-Cre rabies experiments resulted in many more labeled cells at the injection site (Figure 6 B-C, Table S3).

The nuclei receive a massive projection from Purkinje cells, so we first analyzed the distribution of these retrogradely labeled inputs. Notably, the distribution of retrogradely labeled Purkinje cells (PC) differed in location for the two cell types (Figure 6 E, F). PC label following nIntA rabies infection typically appeared in more lateral lobules with most of the rabies labeled cells residing in Cr1 (29.8%), PFl (19.8%), and Cop (16.5%) which, based on anterograde tracing data, also receive direct feedback from nIntA suggesting reciprocal loops. In contrast, the distribution of input to Gad1^{IN} from PCs was more heavily influenced by the intermediate lobules 4/5 (31.6%) and Sim (26.0%). Unsurprisingly, the majority (>60% of all rabies positive cells outside the CbN) of the inputs to both cell types were comprised of ipsilateral PCs (Figure 6F, inlay); however, nIntA received a greater proportion of their total input from the cerebellar cortex than Gad1^{IN}. 3D reconstruction of rabies positive PCs (Figure 6G) showed a highly spatially restricted and organized PC label following sparse nIntA starter label and broadly topographic PC label following iIntA starter label. Extracerebellar input to nIntA was very sparse, while diverse and wide-ranging inputs were labeled following Gad1-cre starter cell label. Both IntA cell types receive input from brain regions related to motor, sensory, or modulatory functions (Figure 6H-I), largely corroborating previous observations with traditional tracers in the cerebellar cortex (Fu et al., 2011). Interestingly, the nIntA neurons were contacted predominately by neurons from motor related regions (93%), while Gad1^{IN} neurons were contacted by neurons from more diverse regions, with motor (74%), sensory (22%), or modulatory (4%; Figure 6I) functions. This patterned mirrored targeting patterns of these cell types. For a complete list of brain regions which provide input to nIntA and iIntA see Table 2 and Figure S5.

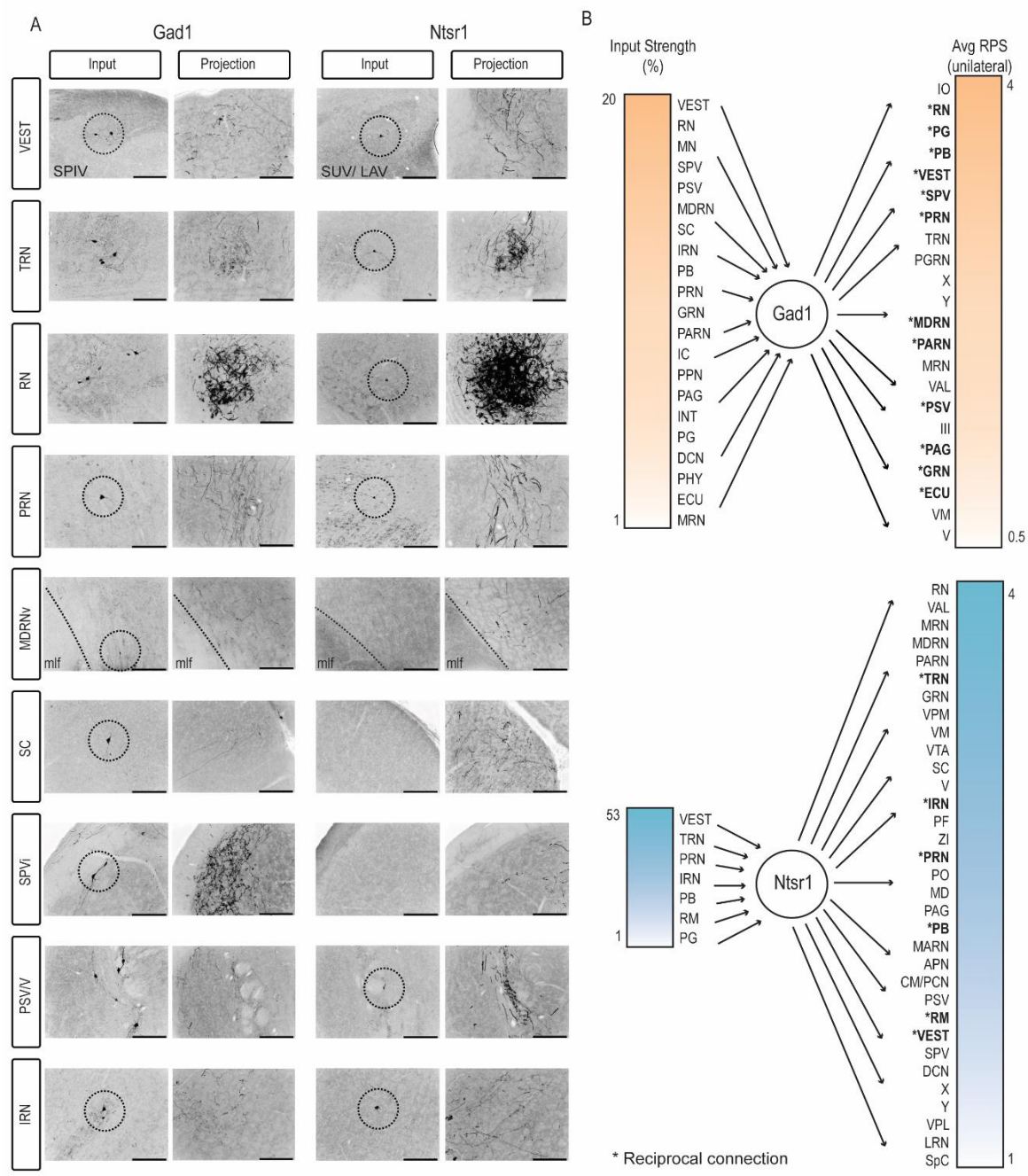

Figure 7. Reciprocal loops between IntA and extracerebellar targets, for both Gad1 and Ntsr1 cells. (A) Images depicting rabies labeled cells (columns 1 and 3, rabies + cells circled if singular or very small) and projections to the same regions at the same coordinates relative to bregma (columns 2 and 4). (B) Inputs and outputs listed in order of increasing percent of rabies labeled cells (left) and relative projection strength (right). Only inputs with greater than 1% of total extracerebellar rabies labeled cells and regions with mean relative projection strengths greater than 1 are listed. Asterisks denote regions that were identified in both retrograde and anterograde tracing.

We observed retrogradely labeled cells from both hemispheres in many regions, although the majority of extracerebellar input neurons to Int reside in the ipsilateral hemisphere. The main extracerebellar projection to nIntA came from VEST (53%), followed by TRN (25%, Schwarz & Schmitz, 1997), PRN (6%), and IRN (5%). A core extracerebellar projection to Gad1^{IN} also came from VEST (20%) and TRN (8%, (Mihailoff, 1993)). However, Gad1^{IN} was also contacted

robustly by RN (8%), MN (8%), SPV (6%), PSV (5%), MDRN (4%), and SC (4%) which in turn receive a projection, apart from MN, from both cell types (Figure 7A, B). We only observed terminal fields in the contralateral MN in a single anterograde tracing Gad1 specimen and 3 of 4 Vgat-restricted specimens, despite the presence of retrogradely labeled cells in the contralateral MN and IN nuclei following a modified rabies injection to the ipsilateral IntA of Gad1-cre mice. Rabies labeled neurons in the contralateral CbN may indicate a cross-hemisphere projection from neurons not genetically defined by Ntsr1 or Gad1. Many canonical sources of mossy fibers, such as ECU, PRN/TRN/PG, LRN (Parenti et al., 1996) were identified as sources of nuclear input as well as recipients of a projection from at least one cell type within IntA. Figure 7 B summarizes the inputs and outputs of both cell types ordered by percentage of rabies labeled cells or RPS. The only IntA brain regions which received a projection but were not also retrogradely labeled were the thalamic nuclei, ZI, APN, PRP, and Nucleus Y.

Discussion

Here we systematically examined the input and output patterns of diverse cell populations of the cerebellar nucleus, IntA, using intersectional viral tracing techniques. Consistent with previous work, we found that the putative excitatory output neurons of IntA collateralize widely to many regions of the contralateral brainstem, spinal cord and thalamus and more restrictedly to the caudal ipsilateral brainstem, including to regions recently shown to control forelimb musculature. However, in contrast to long-standing dogma, we also found that inhibitory GABAergic projection neurons of IntA innervate many brainstem regions including the red nucleus, pontine nuclei, medullary reticular nuclei, and sensory brainstem structures such as SPV and PSV. Interestingly, IO-projecting neurons collateralize to comprise, in part, these projections. Inputs to these distinct cell types were also mapped using monosynaptic rabies tracing. We found that inputs to excitatory neurons of IntA are dominated by PCs and receive predominantly motor-related extracerebellar input. By contrast, inhibitory neurons receive extracerebellar input from a more diverse set of nuclei, including motor, sensory, modulatory, and mixed modality brain regions, in addition to broader PC input. Merging anterograde and retrograde datasets, reciprocal loops between IntA and brainstem targets were common for both cell types.

Among the most surprising results was the widespread ramification of GABAergic neurons of IntA. While such a projection was unknown, these data, combined with previous literature from the medial nucleus, suggest that inhibitory projections from the nuclei may be a more prominent circuit motif than is currently appreciated. The MN contains glycinergic projection neurons that innervate ipsilateral brainstem nuclei matching contralateral targets of excitatory MN neurons (Bagnall et al., 2009). Additional evidence of inhibitory outputs includes dual retrograde tracing suggesting that nucleo-olivary projections from MN and VEST collateralize to the ventromedial hypothalamic nucleus (Diagne et al., 2001; Li et al., 2017). Studies combining retrograde HRP tracing from the basilar pontine nuclei with immunohistochemistry observed double labeled GABA immunopositive neurons in the LN of rats and cats (Aas & Brodal, 1989), although the literature is inconsistent (Schwarz & Schmitz, 1997). More recent work in mice tracing Vgat-cre neurons of the LN listed these projections targeting a variety of brainstem structures as well as IO (Locke et al., 2018), but these results were not discussed. Another study restricting tracer to Sox14-Cre expressing neurons, a transcription factor marking putative nucleo-olivary neurons, showed terminal label in

the IO as well as midbrain structures, but label outside IO was interpreted to reflect tracer leakage to the vestibular nuclei (Prekop et al., 2018). Thus, the limited number of studies to date that have employed Cre-dependent tract tracing from the nuclei, may have resulted in the lack of characterization of these inhibitory projections.

To alleviate concerns that these surprising projections from Gad1-Cre neurons were a consequence of ectopic expression of Cre or other methodological artifact, we challenged the result by employing multiple experimental methods and analyses. First, we used an intersectional approach, targeting Gad1-Cre expressing neurons that project to the IO. This method of isolating inhibitory IntA neurons also consistently labeled terminals elsewhere in the brainstem. Second, we used intersectional methods in a second transgenic mouse line, Vgat-ires-Cre, that also isolates inhibitory neurons. Data from this mouse line were largely consistent with observations in the Gad1-Cre line with several nuanced targeting differences (Table 1). Third, projection patterns of excitatory neurons and intersectional labeled nucleo-olivary projections were different, particularly within the ipsilateral caudal brainstem and diencephalon. Finally, AAV-retroCre injections into RN labeled targets matching mixed projections of excitatory and inhibitory neurons, including terminal label in IO, thus genetic leak of Cre cannot explain the sum of these observations. Despite these corroborating experimental results, we note that our data may appear to contradict conclusions drawn from a dual-retrograde tracing study, in which only minor dual retrograde label was observed in the lateral and interposed nuclei following tracer injections into IO and RN or IO and TRN (Ruigrok & Teune, 2014). This study concluded that two distinct populations exist within the CbN: one which projects widely to several regions and one which projects exclusively to IO. However, this study did report a small number of cells colabeled by retrograde injections to IO and TRN as well as IO and RN. This observation may account for the present finding that a population of neurons which projects to both IO and premotor nuclei exists in smaller numbers, and that topographic specificity may have precluded previous methods from fully detecting the collateralization of inhibitory populations.

Consistent with projection patterns of glycinergic medial and vestibular nucleus neurons, we found that iIntA neurons of the interposed had an ipsilateral projection bias, in contrast to the contralateral bias of nIntA neurons (Bagnall et al., 2009; Prekop et al., 2018; Sekirnjak et al., 2003; Shin et al., 2011). This organizational structure has been proposed to potentially mediate axial muscular opponency. Despite this similarity, the ipsilateral projection bias from iInt was less extreme, with cells of both genotypes projecting bilaterally. Interestingly, IO-projecting Gad1-cre neurons showed a contralateral bias in their projection patterns, while retaining ipsilateral projections. Future studies investigating the functional roles of these projections may explore agonist/antagonist opponency in motor targets of these projections, which remain lateralized for limb musculature. Additionally, the widespread observation of Purkinje neurons that increase rates during cerebellar dependent behaviors may suggest the potential for a double disinhibitory pathway through the nuclei, if these Purkinje neurons converged on inhibitory nuclear output neurons (De Zeeuw, 2020).

Another intriguing distinction between projection targets of distinct cell types was that inhibitory projections targeted more sensory brainstem structures than excitatory outputs. Predicting sensory consequences of self-generated movement, termed forward models, is a leading hypothesis for the role of cerebellum in sensorimotor behaviors. While populations

of Purkinje neurons may perform this computation, it is unknown how forward models are used by downstream targets. Inhibitory projections from cerebellum to sensory areas would seem to be ideally situated to modulate sensory gain of predicted sensory consequences of movement (Brooks et al., 2015; Shadmehr, 2020). Moreover, negative sensory prediction error could be used to actively cancel predicted sensory reafference (Kim et al., 2020; Requarth & Sawtell, 2014; Shadmehr, 2020), raising implications for a combined role of negative sensory prediction error in guiding learning both through modulation of climbing fiber signaling in IO and through modulation of sensory signals reaching the cerebellum upon which associative learning is built.

The present study compliments a recent collection of papers examining cerebellar nuclear cell types. Transcriptomics analyses of the cerebellar nuclei identified three distinct excitatory cell types within IntA. These classes included two broad projection types: those that target a wide array of brainstem nuclei and those that target the ZI (Kebschull et al., 2020). Another recent study identified two distinct interposed cell types based on projection patterns to the spinal cord, which were shown to constitute a minority of neurons (<20%). Nevertheless, these spinal-projecting neurons collateralized to many other targets, including the MDRNv, RN, and the VAL (Sathyamurthy et al., 2020). Inhibitory projections were not examined in these studies, thus it will be interesting to examine how the inhibitory projection neurons identified in the present study map onto transcript clusters of the inhibitory cell types, 5 total across the nuclei. At a minimum, these clusters would include IO-projecting neurons, interneurons, MN glycinergic projection neurons, and a collateralizing population of inhibitory neurons identified here from IntA (Ankri et al., 2015; Bagnall et al., 2009; Fujita et al., 2020; Zoé Husson et al., 2014; Kebschull et al., 2020; Sathyamurthy et al., 2020).

On the input side of these neuronal populations, we observed differences in the input signatures of nIntA and iIntA. nIntA received a greater abundance of PC and motor related precerebellar nuclei input. Other studies have suggested that somatic or dendritic synapses onto large, presumably glutamatergic, neurons of the CbN are largely from PCs (86% or 50% respectively), while MF and CF collaterals form 22% and 5% of synapses onto proximal dendrites (Chan-Palay, 1977; De Zeeuw & Berrebi, 1995; Palkovits et al., 1977). The present results generally substantiate these conclusions with respect to Ntsr1 cells in IntA. PCs composed 87% of nIntA inputs while all other extracerebellar regions composed the remaining 13% of rabies positive neurons. Gad1-Cre neurons in IntA received a higher proportion of extracerebellar inputs (35%) which were more distributed across motor, mixed, sensory, and modulatory precerebellar regions. It remains unclear if there are differences in input connectivity between Gad1+ subgroups, specifically interneurons and projection neurons. In comparing input and outputs to diverse cell types, we noticed that reciprocal loops were common. Previous work from our lab identified loops between the IN and RN (Beitzel et al., 2017). The present data extend that theme to many brainstem structures. Such loops resemble neural integrators used in gaze maintenance or postural limb stabilization (Albert et al., 2020; Cannon & Robinson, 1987), another potential functional role of the anatomy presented here.

These differences in innervation patterns are interesting in light of potentially diverse computations performed by these cell types. The output of IntA is critical to produce precise movements, but how different cell types work in tandem to achieve this goal is unresolved. Dichotomous roles for different cell types have been most clearly hypothesized in delay eyelid

conditioning models, where glutamatergic neurons are proposed to produce the conditioned response while inhibitory neurons regulate the learning 'setpoint' via projections to the IO, the source of climbing fibers (Bengtsson et al., 2007; Garcia & Mauk, 1998; Kim et al., 1998; Kim et al., 2020; McCormick & Thompson, 1984; Medina et al., 2001; Medina et al., 2002; Ten Brinke et al., 2017; Thompson & Steinmetz, 2009). These studies assume that premotor and nucleo-olivary neurons respond in roughly equivalent ways during behavior (Shadmehr, 2020). Differences in the intrinsic and synaptic properties of these neurons, however, raise the likelihood that this prediction may not be realized (Husson et al., 2014; Najac & Raman, 2017; Özcan et al., 2020; Uusisaari & Knöpfel, 2008; Uusisaari et al., 2007; Uusisaari & Knöpfel, 2011). Moreover, our data suggest different cell types also differ in their input sources, further predicting diverse response properties.

In conclusion this study opens the door to many potential functional studies that could explore the roles of inhibitory projections in real-time motor control, sensory prediction and cancellation, and dynamic cerebellar gain control. Taken together, the present results suggest distinct computational modules within the interposed cerebellar nuclei based on cell types and shared, but likely distinct, participation in motor execution.

Materials and Methods

Animals

All procedures followed the National Institutes of Health Guidelines and were approved by the Institutional Animal Care and Use Committee at the University of Colorado Anschutz Medical Campus. Animals were housed in an environmentally controlled room, kept on a 12 h light/dark cycle and had ad libitum access to food and water. Adult mice of either sex were used in all experiments. Genotypes used were C57BL/6 (Charles River Laboratories), Neurotensin receptor1-Cre [Ntsr1-Cre; MutantMouse Regional Resource Center, STOCK Tg(Ntsr1-cre) GN220Gsat/ Mmucd], Gad1-Cre (Higo et al., 2009); Vgat-Cre[#028862]; Jackson Labs]. All transgenic animals were bred on a C57BL/6 background. Gad1 and Ntsr1-Cre mice were maintained as heterozygotes and were genotyped for Cre (Transnetyx). For all surgical procedures, mice were anesthetized with intraperitoneal injections of a ketamine hydrochloride (100 mg/kg) and xylazine (10 mg/kg) cocktail, placed in a stereotaxic apparatus, and prepared for surgery with a scalp incision. For RN injections, craniotomies were made unilaterally above RN (from bregma: 3.5 mm, 0.5 mm lateral, 3.6 mm ventral). For IntA injections, unilateral injections were made at lambda: 1.9 mm posterior, 1.6 mm lateral, 2.1 mm ventral. For IO injections, the mouse's head was clamped facing downward, an incision was made near the occipital ridge, muscle and other tissue was removed just under the occipital ridge, and unilateral injections were made at 0.2 mm lateral, and 2.1 mm ventral with the pipet tilted 10° from the Obex. This method consistently labeled IO and had the advantage of avoiding accidental cerebellar label via pipette leakage.

Viral injections

Injections were administered using a pulled glass pipette. Unilateral pressure injections of 70-200 nl of Cre-dependent reporter viruses (AAV1.CAG.flex.GFP; AAV2.DIO.EF1a.eYFP; AAV8.hysn-ConFon.eYFP, see Resources Table) were made into IntA. Injections were centered on IntA, with minor but unavoidable somatic label appearing in posterior interposed (IntP), lateral nucleus (LN), and the dorsal region of the vestibular (VEST) nuclei. We occasionally

observed minor somatic label in the parabrachial nucleus (PB) and the cerebellar cortex (Cb-Ctx) anterior or dorsal, respectively, to IntA in Gad1 and Vgat injections. In control injections (n = 3; virus in C57/Bl6 mice or off-target injection into Ntsr-1 Cre mice), viral expression was not detected. We did not see appreciable somatic label in the medial nucleus (MN) of any specimens. To achieve restricted injection sites, smaller volumes were required in Gad1-cre/Vgat-cre mice compared to Ntsr1-cre mice (70-100 nL vs 150-200 nL, respectively). Retrograde labeling of RN-projecting IntA neurons was achieved through AAVretro-EF1a-cre (Tervo et al., 2016). Retrograde injections of RN were performed simultaneously with flex-GFP injections of IntA. Retrograde virus (AAVretro-EF1a-Flp) was injected to IO one week before reporter viruses because of the different targeting scheme and mice were allowed to heal one week prior to the reporter virus injection. All mice injected with AAVs were housed postoperatively for 5 – 6 weeks before perfusion to allow for viral expression throughout the entirety of the axonal arbor. Control injections were performed where Cre or Flp expression was occluded, either by performing the injections in wild type mice or in transgenic mice without the Retro-flp injection into IO or RN, confirming the necessity of recombinase presence in reporter expression (Fenno et al., 2017).

For monosynaptic rabies retrograde tracing, AAV1.EF1.Flex.TVA.mCherry (University of North Carolina Vector Core; (Watabe-Uchida et al., 2012)) and AAV9.Flex.H2B.GFP.2A.oG (Salk Gene Transfer, Targeting and Therapeutics Core; (E. J. Kim et al., 2016)) were co-injected (100 nL of each; vortexed together) unilaterally into IntA of Gad1-Cre and Ntsr1-cre mice. After a 4-6-week incubation period, a second injection of EnvA.SADΔG.eGFP virus (150-200 nL) was made at the same location (Salk Gene Transfer, Targeting and Therapeutics Core; (E. J. Kim et al., 2016; Wall et al., 2010; Wickersham et al., 2007). Mice were sacrificed a week following the rabies injection and prepared for histological examination.

Tissue Preparation and imaging

Mice were overdosed with an intraperitoneal injection of a sodium pentobarbital solution, Fatal Plus (MWI), and perfused transcardially with 0.9% saline followed by 4% paraformaldehyde in 0.1 M phosphate buffer. Brains were removed and postfixed for at least 24 hours then cryoprotected in 30% sucrose for at least 24 hours. Tissue was sliced in 40 µm consecutive coronal sections using a freezing microtome and stored in 0.1 M phosphate buffer. Every section for rabies experiments and every third section for anterograde tracing experiments was mounted onto slides and imaged. Spinal cord sections were also sliced in 40 µm consecutive coronal sections with every 4th section mounted. Slides were imaged at 10x using a Keyence BZX-800 microscope or a slide-scanning microscope (Leica DM6000BEpifluorescence & Brightfield Slide Scanner; Leica HC PL APO 10x Objective with a 0.4 numerical aperture; Objective Imaging Surveyor, V7.0.0.9 MT). Images were converted to TIFF files (OIViewer Application V9.0.2.0) and analyzed or adjusted via pixel intensity histograms in Image J. We inverted fluorescence images using greyscale lookup tables in order to illustrate results more clearly.

Analysis of overlap by genetically defined neurons

To distinguish overlap of Cre expression with transmitter markers, we analyzed expression data publicly available from the Allen Brain Atlas transgenic characterization, experiments (Ntsr1 vs Gad1) 81582764 and 81747432; (Vglut2 vs Vgat) 304863737; (Vgat vs Gad1) expt #100142488 We applied a threshold to the two fluorescent channels (GFP driven by a transgenic Cre line and RFP via fluorescent *in situ* hybridization (FISH) staining). We then quantified the percentage of

pixel coordinates within Int where fluorescence was detected in both channels (Figure S1A-B). These images are publicly available from: https://connectivity.brain-map.org/transgenic.

Cell size analysis

We imaged cells within IntA at 20x then used the "Measure" tool in ImageJ to gather the cross-sectional area and the "Fit ellipse" measurement to gather minimum and maximum diameter which we converted from pixels to microns using reference scale bars. We report the maximum diameter. We analyzed 15-110 well focused and isolated cells for each specimen.

Brain region classification

We used a combination of the Allen Mouse Brain Reference Atlas and the *Mouse Brain in Stereotaxic Coordinates* by Franklin and Paxinos to identify brain regions, while noting that there were minor differences in location, shape and naming of the brain regions between these reference sources (Lein et al., 2007; Franklin & Paxinos, 2008). In general, we followed nomenclature and coordinates respective to bregma following the Allen Mouse Brain Reference Atlas including its classification conventions of motor, sensory, modulatory sources from the 2008 version. Thalamic regions were classified as motor if they project to motor cortices; sensory if they project to sensory cortices, with intralaminar thalamic nuclei classified as modulatory. The intermediate and deep layers of the superior colliculus harbored terminal fields and retrogradely labeled neurons and is thus classified as motor. For cerebellar nuclear subdivisions, we used the Franklin and Paxinos Atlas. We generally grouped the dorsolateral and anterior subdivisions of the IN because they were often co-labeled, are difficult to confidently distinguish, and occur at similar anterior-posterior (AP) coordinates. We classified somatic reporter protein positive neurons ventral to the three main CbN (IN, LN, MN) and superior cerebellar peduncle (SCP) as being located within the vestibular nuclei (VEST). This region includes the superior, lateral, and medial VEST, as well as a 'vestibular cerebellar' nucleus defined by the *Mouse Brain in Stereotaxic Coordinates* by Franklin and Paxinos but excludes the spinal subdivision. In addition, for simplicity, we grouped regions with many subdivisions or that were depicted with unclear boundaries in *Mouse Brain in Stereotaxic Coordinates* by Franklin and Paxinos as seen in the Allen Brain Atlas (e.g. zona incerta, ZI, and fields of forrel, FF).

Projection quantification

Following viral incubation periods, we mapped terminals to a collection of extracerebellar targets spanning the anterior-posterior (A-P) axis from the posterior medulla to the thalamus. We assigned terminal fields a relative projection strength (RPS) of 0-4 based on the density and anterior-posterior spread (Table 1). The values were assigned relative to the highest density projection target for each genotype: All Ntsr1-Cre projection fields were assigned relative to the density of terminals in RN whereas Gad1-Cre and Vgat-Cre specimens were assigned relative to the density of IO terminals (Figure S1C). Briefly, a terminal field that was both dense and broad (in spanning the anterior-posterior axis) was assigned a relative projection strength (RPS) of 4, semi-dense and semi-broad assigned a 3, semi-dense and/ or semi-broad a 2, and fields determined to be neither dense nor broad but nevertheless present, were assigned an RPS of 1. In addition, we compared our specimens to analogous preparations published in the Allen Mouse Brain Connectivity Atlas, specifically the histological profile of Cre-dependent labeling following injections into IntA of either Ntsr1-Cre or Slc32a1(Vgat)-ires-Cre mice. These publicly available sources recapitulated projection signatures from lab specimen (Table S1). We

included the Allen injection data in our analysis of average projection strength for Ntsr1-Cre (n=1) and Vgat-Cre (n=1) specimen but did not use the histological images of these injections here. The full histological profiles of genetically restricted GFP label from the Allen can be found at: 2011 Allen Institute for Brain Science. Mouse Brain Connectivity Atlas. Available from: http://connectivity.brain-map.org/, experiments #264096952, #304537794.

Rabies quantification

We identified presumptive starter cells as *rabies positive cells* within the cerebellar nuclei where both mCherry (AAV1.EF1.Flex.TVA.mCherry) and GFP (AAV9.Flex.H2B.GFP.2A.oG.GFP/ EnvA.SADΔG.eGFP) were expressed. We could not easily identify cells in which all three components were present due to overlapping fluorescence from the oG and modified rabies viruses, thus starter cell identification is an estimate. An additional caveat is that we are unable to distinguish starter cells from local interneurons infected transsynaptically which may artificially inflate the number of starter cells. While we occasionally observed oG expression in GABAergic Purkinje cells (PC), Golgi cells (GoC), and molecular layer interneurons (MLIs) in Gad1-cre mice, TVA was rarely expressed in these areas, precluding direct infection with rabies virus. Consistent with this, we looked for but did not observe granule cell (GrC) label, effectively suggesting a lack of transcomplementation in the cerebellar cortex.

Abbreviations:

APN- Anterior Pretectal Nucleus
B- Barrington's Nucleus
CbCtx- Cerebellar Cortex
CbN- Cerebellar Nuclei
CM- Centromedial nucleus of the thalamus
CN- Cochlear Nucleus
CUN- Cuneate Nucleus
DCN- Dorsal Column Nucleus
DTN- Dorsal Tegmental Nucleus
ECU- External Cuneate Nucleus
GoC- Golgi Cells
GRN- Gigantocellular Reticular Nucleus
IC- Inferior Colliculus
III- Occulomotor Nucleus
IN- Interposed Nucleus
IntA- Anterior Interposed Nucleus
IO- Inferior Olive
IRN- Intermediate reticular nucleus
LC- Locus Ceruleus
LDT- Lateral dorsal tegmental nucleus
LN- Lateral Cerebellar Nucleus
LRN- Lateral Reticular Nucleus
MARN- Magnocellular reticular nucleus
MD- Mediodorsal nucleus of the thalamus
MDRNd- Medullary reticular nucleus-dorsal
MDRNv - Medullary reticular nucleus-ventral
MLI- Molecular Layer Interneurons
MN- Medial Cerebellar Nucleus
MRN- Midbrain reticular nucleus
NLL- nucleus of the lateral lemniscus
NTS- Nucleus of the solitary tract
P5- Peritrigeminal nucleus
PAG- Periaqueductal grey
PARN- Parvicellular reticular nucleus
PAS- Parasolitary nucleus
PB- Parabrachial nuclei
PC- Purkinje Cells
PCG- Pontine Central Gray
PCN- Paracentral nucleus of the thalamus
PDTg- Posterodrosal tegmental nucleus
PF - Parafascicular nucleus of the thalamus
PG- Pontine gray
PGRN - Paragigantocellular reticular nucleus
PHY- Perihypoglossal nuclei
PMR- Paramedian reticular nucleus
PO- Posterior complex of the thalamus

PPN - Pedunculopontine nucleus
PPY- Parapyramidal nucleus
PRN- Pontine reticular nucleus
PRP- Prepositus nucleus
PRT- Pretectal region
PSV- Principal sensory nucleus of the trigeminal
RAmb- Midbrain raphe nucleus
RM- Nucleus raphe magnus
RN- Red nucleus
RPS- Relative Projection Strength
SAG- Nucleus sagulum
SC- Superior colliculus
SLC- Subceruleus nucleus
SLD- Sublaterodorsal nucleus
SNr- Substantia nigra, reticulata
SPVc- Spinal nucleus of the trigeminal, caudal
SPVi- Spinal nucleus of the trigeminal, interpolar
SPVo- Spinal nucleus of the trigeminal, oral
SUT- Supratrigeminal nucleus
TRN- Tegmental reticular nucleus of the pons
V- Motor nucleus of the trigeminal
VAL- Ventral anterior-lateral complex of the thalamus
VEST- Vestibular nuclei
VII- Facial motor nucleus
VM- Ventral medial nucleus of the thalamus
VPL- Ventral posterolateral nucleus of the thalamus
VPM- Ventral posteromedial nucleus of the thalamus
VTA- Ventral tegmental area
X- Nucleus X
XII- Hypoglossal nucleus
Y- Nucleus Y
ZI- Zona incerta

References:

Aas, J.-E., & Brodal, P. (1989). Demonstration of a Mamillo-Ponto-Cerebellar Pathway. *The European Journal of Neuroscience*, *1*(1), 61–74.

Albert, S. T., Hadjiosif, A. M., Jang, J., Zimnik, A. J., Soteropoulos, D. S., Baker, S. N., Churchland, M. M., Krakauer, J. W., & Shadmehr, R. (2020). Postural control of arm and fingers through integration of movement commands. *ELife*, *9*.

Ankri, L., Husson, Z., Pietrajtis, K., Proville, R., Léna, C., Yarom, Y., Dieudonné, S., & Uusisaari, M. Y. (2015). A novel inhibitory nucleo-cortical circuit controls cerebellar Golgi cell activity. *ELife*, *4*.

Aumann, T. D., Rawson, J. A., Finkelstein, D. I., & Horne, M. K. (1994). Projections from the lateral and interposed cerebellar nuclei to the thalamus of the rat: A light and electron microscopic study using single and double anterograde labelling. *The Journal of Comparative Neurology*, *349*(2), 165–181.

Bagnall, M. W., Zingg, B., Sakatos, A., Moghadam, S. H., Zeilhofer, H. U., & Lac, S. du. (2009). Glycinergic Projection Neurons of the Cerebellum. *Journal of Neuroscience*, *29*(32), 10104–10110.

Batini, C., Compoint, C., Buisseret-Delmas, C., Daniel, H., & Guegan, M. (1992). Cerebellar nuclei and the nucleocortical projections in the rat: Retrograde tracing coupled to GABA and glutamate immunohistochemistry. *Journal of Comparative Neurology*, *315*(1), 74–84.

Becker, M. I., & Person, A. L. (2019). Cerebellar Control of Reach Kinematics for Endpoint Precision. *Neuron*, *103*(2), 335-348.e5.

Beitzel, C. S., Houck, B. D., Lewis, S. M., & Person, A. L. (2017). Rubrocerebellar Feedback Loop Isolates the Interposed Nucleus as an Independent Processor of Corollary Discharge Information in Mice. *The Journal of Neuroscience*, *37*(42), 10085–10096.

Bengtsson, F., Jirenhed, D.-A., Svensson, P., & Hesslow, G. (2007). Extinction of conditioned blink responses by cerebello-olivary pathway stimulation. *Neuroreport*, *18*(14), 1479–1482.

Brooks, J. X., Carriot, J., & Cullen, K. E. (2015). Learning to expect the unexpected: Rapid updating in primate cerebellum during voluntary self-motion. *Nature Neuroscience*, *18*(9), 1310–1317.

Cannon, S. C., & Robinson, D. A. (1987). Loss of the neural integrator of the oculomotor system from brain stem lesions in monkey. *Journal of Neurophysiology*, *57*(5), 1383–1409.

Canto, C. B., Witter, L., & De Zeeuw, C. I. (2016). Whole-Cell Properties of Cerebellar Nuclei Neurons In Vivo. *PloS One*, *11*(11), e0165887.

Carta, I., Chen, C. H., Schott, A. L., Dorizan, S., & Khodakhah, K. (2019). Cerebellar modulation of the reward circuitry and social behavior. *Science (New York, N.Y.)*, *363*(6424). 1

Chan-Palay, V. (1977). The Cerebellar Dentate Nucleus. In V. Chan-Palay (Ed.), *Cerebellar Dentate Nucleus: Organization, Cytology and Transmitters* (pp. 1–24). Springer.

Chen, C. H., Fremont, R., Arteaga-Bracho, E. E., & Khodakhah, K. (2014). Short latency cerebellar modulation of the basal ganglia. *Nature Neuroscience*, *17*(12), 1767–1775.

Cooper, S. E., Martin, J. H., & Ghez, C. (2000). Effects of inactivation of the anterior interpositus nucleus on the kinematic and dynamic control of multijoint movement. *Journal of Neurophysiology*, *84*(4), 1988–2000.

De Zeeuw, C. I., & Berrebi, A. S. (1995). Postsynaptic targets of Purkinje cell terminals in the cerebellar and vestibular nuclei of the rat. *The European Journal of Neuroscience*, *7*(11), 2322–2333.

De Zeeuw, Chris I. (2020). Bidirectional learning in upbound and downbound microzones of the cerebellum. *Nature Reviews. Neuroscience*.

Diagne, M., Delfini, C., Angaut, P., Buisseret, P., & Buisseret-Delmas, C. (2001). Fastigiovestibular projections in the rat: Retrograde tracing coupled with gammaamino-butyric acid and glutamate immunohistochemistry. *Neuroscience Letters*, *308*(1), 49–53.

Doykos, T. K., Gilmer, J. I., Person, A. L., & Felsen, G. (2020). Monosynaptic inputs to specific cell types of the intermediate and deep layers of the superior colliculus. *Journal of Comparative Neurology*, *528*(13), 2254–2268.

Dumas, D. B., Gornati, S. V., Adolfs, Y., Shimogori, T., Pasterkamp, R. J., & Hoebeek, F. E. (2019). Anatomical development of the cerebellothalamic tract in embryonic mice. *BioRxiv*, 731968.

Esposito, M. S., Capelli, P., & Arber, S. (2014). Brainstem nucleus MdV mediates skilled forelimb motor tasks. *Nature*, *508*(7496), 351–356.

Fenno, L. E., Mattis, J., Ramakrishnan, C., & Deisseroth, K. (2017). A Guide to Creating and Testing New INTRSECT Constructs. *Current Protocols in Neuroscience*, *80*, 4.39.1-4.39.24.

Fenno, L. E., Mattis, J., Ramakrishnan, C., Hyun, M., Lee, S. Y., He, M., Tucciarone, J., Selimbeyoglu, A., Berndt, A., Grosenick, L., Zalocusky, K. A., Bernstein, H., Swanson, H., Perry, C., Diester, I., Boyce, F. M., Bass, C. E., Neve, R., Huang, Z. J., & Deisseroth, K. (2014). Targeting cells with single vectors using multiple-feature Boolean logic. *Nature Methods*, *11*(7), 763–772.

Fredette, B. J., & Mugnaini, E. (1991). The GABAergic cerebello-olivary projection in the rat. *Anatomy and Embryology*, *184*(3), 225–243.

Fu, Y., Tvrdik, P., Makki, N., Paxinos, G., & Watson, C. (2011). Precerebellar Cell Groups in the Hindbrain of the Mouse Defined by Retrograde Tracing and Correlated with Cumulative Wnt1-Cre Genetic Labeling. *The Cerebellum*, *10*(3), 570. 1

Fujita, H., Kodama, T., & du Lac, S. (2020). Modular output circuits of the fastigial nucleus for diverse motor and nonmotor functions of the cerebellar vermis. *ELife*, *9*.

Gao, Z., Proietti-Onori, M., Lin, Z., ten Brinke, M. M., Boele, H.-J., Potters, J.-W., Ruigrok, T. J. H., Hoebeek, F. E., & De Zeeuw, C. I. (2016). Excitatory Cerebellar Nucleocortical Circuit Provides Internal Amplification during Associative Conditioning. *Neuron*, *89*(3), 645–657.

Garcia, K. S., & Mauk, M. D. (1998). Pharmacological analysis of cerebellar contributions to the timing and expression of conditioned eyelid responses. *Neuropharmacology*, *37*(4–5), 471–480.

Gayer, N. S., & Faull, R. L. (1988). Connections of the paraflocculus of the cerebellum with the superior colliculus in the rat brain. *Brain Research*, *449*(1–2), 253–270.

Gong, S., Doughty, M., Harbaugh, C. R., Cummins, A., Hatten, M. E., Heintz, N., & Gerfen, C. R. (2007). Targeting Cre recombinase to specific neuron populations with bacterial artificial

chromosome constructs. *The Journal of Neuroscience: The Official Journal of the Society for Neuroscience*, *27*(37), 9817–9823.

Higo, S., Akashi, K., Sakimura, K., & Tamamaki, N. (2009). Subtypes of GABAergic neurons project axons in the neocortex. *Frontiers in Neuroanatomy*, *3*9

Houck, B. D., & Person, A. L. (2015). Cerebellar Premotor Output Neurons Collateralize to Innervate the Cerebellar Cortex. *The Journal of Comparative Neurology*, *523*(15), 2254–2271.

Husson, Z., Rousseau, C. V., Broll, I., Zeilhofer, H. U., & Dieudonne, S. (2014). Differential GABAergic and Glycinergic Inputs of Inhibitory Interneurons and Purkinje Cells to Principal Cells of the Cerebellar Nuclei. *Journal of Neuroscience*, *34*(28), 9418–9431.

Husson, Z, Rousseau, C. V., Broll, I., Zeilhofer, H. U., & Dieudonné, S. (2014). Differential GABAergic and Glycinergic Inputs of Inhibitory Interneurons and Purkinje Cells to Principal Cells of the Cerebellar Nuclei. *The Journal of Neuroscience*, *34*(28), 9418–9431.

Ikai, Y., Takada, M., Shinonaga, Y., & Mizuno, N. (1992). Dopaminergic and non-dopaminergic neurons in the ventral tegmental area of the rat project, respectively, to the cerebellar cortex and deep cerebellar nuclei. *Neuroscience*, *51*(3), 719–728.

Kalil, K. (1981). Projections of the cerebellar and dorsal column nuclei upon the thalamus of the rhesus monkey. *Journal of Comparative Neurology*, *195*(1), 25–50.

Kebschull, J. M., Richman, E. B., Ringach, N., Friedmann, D., Albarran, E., Kolluru, S. S., Jones, R. C., Allen, W. E., Wang, Y., Cho, S. W., Zhou, H., Ding, J. B., Chang, H. Y., Deisseroth, K., Quake, S. R., & Luo, L. (2020). Cerebellar nuclei evolved by repeatedly duplicating a conserved cell-type set. *Science*, *370*(6523).

Kim, E. J., Jacobs, M. W., Ito-Cole, T., & Callaway, E. M. (2016). Improved Monosynaptic Neural Circuit Tracing Using Engineered Rabies Virus Glycoproteins. *Cell Reports*, *15*(4), 692–699.

Kim, J. J., Krupa, D. J., & Thompson, R. F. (1998). Inhibitory cerebello-olivary projections and blocking effect in classical conditioning. *Science (New York, N.Y.)*, *279*(5350), 570–573.

Kim, O. A., Ohmae, S., & Medina, J. F. (2020). A cerebello-olivary signal for negative prediction error is sufficient to cause extinction of associative motor learning. *Nature Neuroscience*, 1–5.

Lein, E. S., Hawrylycz, M. J., Ao, N., Ayres, M., Bensinger, A., Bernard, A., Boe, A. F., Boguski, M. S., Brockway, K. S., Byrnes, E. J., Chen, L., Chen, L., Chen, T.-M., Chi Chin, M., Chong, J., Crook, B. E., Czaplinska, A., Dang, C. N., Datta, S., … Jones, A. R. (2007). Genome-wide atlas of gene expression in the adult mouse brain. *Nature*, *445*(7124), 168–176.

Li, B., Zhuang, Q.-X., Gao, H.-R., Wang, J.-J., & Zhu, J.-N. (2017). Medial cerebellar nucleus projects to feeding-related neurons in the ventromedial hypothalamic nucleus in rats. *Brain Structure and Function*, *222*(2), 957–971.

Locke, T. M., Soden, M. E., Miller, S. M., Hunker, A., Knakal, C., Licholai, J. A., Dhillon, K. S., Keene, C. D., Zweifel, L. S., & Carlson, E. S. (2018). Dopamine D1 receptor positive neurons in the lateral nucleus of the cerebellum contribute to cognitive behavior. *Biological Psychiatry*, *84*(6), 401–412.

Low, A. Y. T., Thanawalla, A. R., Yip, A. K. K., Kim, J., Wong, K. L. L., Tantra, M., Augustine, G. J., & Chen, A. I. (2018). Precision of Discrete and Rhythmic Forelimb Movements Requires a Distinct Neuronal Subpopulation in the Interposed Anterior Nucleus. *Cell Reports*, *22*(9), 2322–2333.

McCormick, D. A., & Thompson, R. F. (1984). Neuronal responses of the rabbit cerebellum during acquisition and performance of a classically conditioned nictitating membrane-eyelid response. *The Journal of Neuroscience: The Official Journal of the Society for Neuroscience*, *4*(11), 2811–2822.

Medina, J. F., Garcia, K. S., & Mauk, M. D. (2001). A mechanism for savings in the cerebellum. *The Journal of Neuroscience: The Official Journal of the Society for Neuroscience*, *21*(11), 4081–4089.

Medina, Javier F., Nores, W. L., & Mauk, M. D. (2002). Inhibition of climbing fibres is a signal for the extinction of conditioned eyelid responses. *Nature*, *416*(6878), 330–333.

Mihailoff, G. A. (1993). Cerebellar nuclear projections from the basilar pontine nuclei and nucleus reticularis tegmenti pontis as demonstrated with PHA-L tracing in the rat. *The Journal of Comparative Neurology*, *330*(1), 130–146.

Najac, M., & Raman, I. M. (2017). Synaptic excitation by climbing fibre collaterals in the cerebellar nuclei of juvenile and adult mice. *The Journal of Physiology*, *595*(21), 6703–6718.]

Özcan, O. O., Wang, X., Binda, F., Dorgans, K., De Zeeuw, C. I., Gao, Z., Aertsen, A., Kumar, A., & Isope, P. (2020). Differential Coding Strategies in Glutamatergic and GABAergic Neurons in the Medial Cerebellar Nucleus. *The Journal of Neuroscience: The Official Journal of the Society for Neuroscience*, *40*(1), 159–170.

Palkovits, M., Mezey, É., Hámori, J., & Szentágothai, J. (1977). Quantitative histological analysis of the cerebellar nuclei in the cat. I. Numerical data on cells and on synapses. *Experimental Brain Research*, *28*(1), 189–209.

Parenti, R., Cicirata, F., Pantò, M. R., & Serapide, M. F. (1996). The projections of the lateral reticular nucleus to the deep cerebellar nuclei. An experimental analysis in the rat. *The European Journal of Neuroscience*, *8*(10), 2157–2167.

Franklin, K. B. J. F., MA, & Paxinos, G. (2008). *The Mouse Brain in Stereotaxic Coordinates, Compact: The Coronal Plates and Diagrams*. Elsevier Science.

Prekop, H.-T., Kroiss, A., Rook, V., Zagoraiou, L., Jessell, T. M., Fernandes, C., Delogu, A., & Wingate, R. J. T. (2018). Sox14 Is Required for a Specific Subset of Cerebello–Olivary Projections. *Journal of Neuroscience*, *38*(44), 9539–9550.

Requarth, T., & Sawtell, N. B. (2014). Plastic corollary discharge predicts sensory consequences of movements in a cerebellum-like circuit. *Neuron*, *82*(4), 896–907.

Ruigrok, T. J. H., & Teune, T. M. (2014). Collateralization of cerebellar output to functionally distinct brainstem areas. A retrograde, non-fluorescent tracing study in the rat. *Frontiers in Systems Neuroscience*, *8*.

Sathyamurthy, A., Barik, A., Dobrott, C. I., Matson, K. J. E., Stoica, S., Pursley, R., Chesler, A. T., & Levine, A. J. (2020). Cerebellospinal Neurons Regulate Motor Performance and Motor Learning. *Cell Reports*, *31*(6), 107595.

Schwarz, C., & Schmitz, Y. (1997). Projection from the cerebellar lateral nucleus to precerebellar nuclei in the mossy fiber pathway is glutamatergic: A study combining anterograde tracing with immunogold labeling in the rat. *The Journal of Comparative Neurology*, *381*(3), 320–334.

Sekirnjak, C., Vissel, B., Bollinger, J., Faulstich, M., & du Lac, S. (2003). Purkinje cell synapses target physiologically unique brainstem neurons. *The Journal of Neuroscience: The Official Journal of the Society for Neuroscience*, *23*(15), 6392–6398.

Shadmehr, R. (2020). Population coding in the cerebellum: A machine learning perspective. *Journal of Neurophysiology*, *124*(6), 2022–2051. 0

Shin, M., Moghadam, S. H., Sekirnjak, C., Bagnall, M. W., Kolkman, K. E., Jacobs, R., Faulstich, M., & Lac, S. du. (2011). Multiple Types of Cerebellar Target Neurons and Their Circuitry in the Vestibulo-ocular Reflex. *Journal of Neuroscience*, *31*(30), 10776–10786.

Stanton, G. B. (1980). Topographical organization of ascending cerebellar projections from the dentate and interposed nuclei in Macaca mulatta: An anterograde degeneration study. *The Journal of Comparative Neurology*, *190*(4), 699–731.

Sugimoto, T., Mizuno, N., & Uchida, K. (1982). Distribution of cerebellar fiber terminals in the midbrain visuomotor areas: An autoradiographic study in the cat. *Brain Research*, *238*(2), 353–370.

Ten Brinke, M. M., Heiney, S. A., Wang, X., Proietti-Onori, M., Boele, H.-J., Bakermans, J., Medina, J. F., Gao, Z., & De Zeeuw, C. I. (2017). Dynamic modulation of activity in cerebellar nuclei neurons during pavlovian eyeblink conditioning in mice. *ELife*, *6*.

Teune, T. M., Burg, J. van der, Zeeuw, C. I. de, Voogd, J., & Ruigrok, T. J. H. (1998). Single Purkinje cell can innervate multiple classes of projection neurons in the cerebellar nuclei of the rat: A light microscopic and ultrastructural triple-tracer study in the rat. *Journal of Comparative Neurology*, *392*(2), 164–178.

Thompson, R. F., & Steinmetz, J. E. (2009). The role of the cerebellum in classical conditioning of discrete behavioral responses. *Neuroscience*, *162*(3), 732–755.

Tolbert, D. L., Bantli, H., & Bloedel, J. R. (1978). Organizational features of the cat and monkey cerebellar nucleocortical projection. *The Journal of Comparative Neurology*, *182*(1), 39–56.

Turecek, J., & Regehr, W. G. (2020). Cerebellar and vestibular nuclear synapses in the inferior olive have distinct release kinetics and neurotransmitters. *ELife*, *9*.

Uusisaari, M., & Knöpfel, T. (2008). GABAergic synaptic communication in the GABAergic and non-GABAergic cells in the deep cerebellar nuclei. *Neuroscience*, *156*(3), 537–549.

Uusisaari, M., & Knöpfel, T. (2010). GlyT2+ neurons in the lateral cerebellar nucleus. *Cerebellum (London, England)*, *9*(1), 42–55.

Uusisaari, M,, & Knöpfel, T. (2011). Functional Classification of Neurons in the Mouse Lateral Cerebellar Nuclei. *The Cerebellum*, *10*(4), 637–646.

Uusisaari, Marylka, Obata, K., & Knöpfel, T. (2007). Morphological and Electrophysiological Properties of GABAergic and Non-GABAergic Cells in the Deep Cerebellar Nuclei. *Journal of Neurophysiology*, *97*(1), 901–911.

Vong, L., Ye, C., Yang, Z., Choi, B., Chua, S., & Lowell, B. B. (2011). Leptin action on GABAergic neurons prevents obesity and reduces inhibitory tone to POMC neurons. *Neuron*, *71*(1), 142–154.

Wall, N. R., Wickersham, I. R., Cetin, A., De La Parra, M., & Callaway, E. M. (2010). Monosynaptic circuit tracing in vivo through Cre-dependent targeting and complementation of modified rabies virus. *Proceedings of the National Academy of Sciences of the United States of America*, *107*(50), 21848–21853.

Watabe-Uchida, M., Zhu, L., Ogawa, S. K., Vamanrao, A., & Uchida, N. (2012). Whole-brain mapping of direct inputs to midbrain dopamine neurons. *Neuron*, *74*(5), 858–873.

Wickersham, I. R., Lyon, D. C., Barnard, R. J. O., Mori, T., Finke, S., Conzelmann, K.-K., Young, J. A. T., & Callaway, E. M. (2007). Monosynaptic Restriction of Transsynaptic Tracing from Single, Genetically Targeted Neurons. *Neuron*, *53*(5), 639–647.

Wickersham, I. R., Sullivan, H. A., & Seung, H. S. (2010). Production of glycoprotein-deleted rabies viruses for monosynaptic tracing and high-level gene expression in neurons. *Nature Protocols*, *5*(3), 595–606

Acknowledgments:

We thank Courtney Dobrott for sharing expertise in spinal cord removal and Aya Miften for assistance in histology. We are grateful to Dr Jason Aoto for preparation of AAVRetro viruses. This work was supported by NS114430, NSF CAREER 1749568, and by a grant from the Simons Foundation as part of the Simons-Emory International Consortium on Motor Control. Imaging of rabies label was performed in the Advanced Light Microscopy Core, part of the NeuroTechnology Center at University of Colorado Anschutz Medical Campus supported in part by Rocky Mountain Neurological Disorders Core Grant Number P30 NS048154 and by Diabetes Research Center Grant Number P30 DK116073. Rabies viruses were obtained from the Salk GT3 Core Facility of supported by NIH-NCI CCSG: P30 014195, an NINDS R24 Core Grant and funding from NEI.

Table 1. Anterograde tracing summary. Average RPS for all specimens in Ntsr1-Cre (n = 6; including Allen specimen), Ntsr1RN (n = 4), RNRetroCre (n = 3), Gad1-Cre (n = 5), Gad1IO (n = 4), Vgat (n = 4, including Allen specimen), and VgatIO (n = 3). RPS depicted as symbols (+ for contralateral RPS, O for ipsilateral RPS). One symbol = avg RPS < 1, two symbols = avg RPS ≥ 1 and <2, three symbols = avg RPS ≥2 and <3, four symbols = avg RPS ≥ 3.

Brain Region	Ntsr1	Ntsr1-RN	RN-Cre	Gad1	Gad1-IO	Vgat	Vgat-IO

Motor							
RN	+ + + +	+ + + +	+ + + +	+ +	+ + +	+ +	+ +
						o o	o o
VAL	+ + + +	+ + + +	+ + +	+	+ +		
	o	o					
MRN	+ + ++	+ + + +	+ + +	+	+ + +	+	
	o		o	o	o	o	o
TRN	+ + + +	+ + + +	+ + + +	+	+ + +	+ +	+ +
						o	o
VM	+ + +	+ + +	+ + +	+	+ + +		
					o	o	
PRN	+ + +	+ +	+ + +	+	+ +	+ +	+ +
			o	o	o	o o	o o
SC	+ + +	+ +	+ + +	+	+ +		
						o	
GRN	+ + +	+ +	+ +	+	+ +	+	+
	o	o	o	o	o	o o	o o o
MDRNv	+ + +	+ +	+ + +		+ +	+	+
	o	o		o	o	o o	o o
PAG	+ + +	+ +	+ +		+ +	+	
	o	o	o	o	o	o o	o o
APN	+ +		+ +			+	
MARN	+ +	+ +	+ +		+	+	+
						o	o
LRN	+ +	+		o	+	+ +	
	o		o o		o	o o	o
SpC	+ +	++	N/A				
PG	+	+		+ +	+	+ + +	+ + +
				o		o o o	o o
IRN	+				+		
	o o o	o o	o o o	o	o o	o o	
PARN	+				+		
	o o o o	o o o	o o o	o o	o o o	o o	o
MDRNd	+				+	+	
	o o o o	o o o	o o o o	o o	o o o	o o	o
VEST	+	+	++	+	+	+ +	+
	o o	o o	o o	o o	o o	o o o o	o o o
Y	+			o		+	
	o o	o	o			o o o	o
SUT					+		
	o	o			o		
X						+	+
	o o	o	o o	o o	o	o o o	o
V						+	
	o o o	o o	o o	o	o o	o o	
IO	+		+ + +	+ + + +	+ + + +	+ + + +	+ + + +
				o o	o	o o o	o o o
RPP	+						
						o o	
PGRN						+	+
				o o	o	o o o	o o
III							
				o	o	o o	o
XII						+	+
				o		o o	o o

VII						+ o	
MN				+		+	+
Mixed							
ZI	+ + +	+ +	+ +		+ + o	+ o o	o
Sensory							
VPM	+ +	+	+ + +	+		o	o
VPL	+ +	+	+				
ECU			+ o o	o	+	+ + o o o	+ o
DCN	+ o o	o	+ + o	+ o	+ o o	+ o o o	+ o o
SPVi	o	o	o o	o o	o o	+ o o o	+ o o
SPVo	o o	o o	o o	o o	o o	+ o o	
SPVc				o		+ o o	o
PB	o o	o o	o o	+ o o	+ o o	+ + o o o	+ o
PSV	o o	o	o o	o	o o	+ o o o	
NTS	+ o			o		+ + o o o	+ o
Modulatory							
VTA	+ + +	+ +	+ + +		+ +	+	
PF	+ + +	+ +	+ + +		+ +	+	
MD	+ + +	+	+ + +	o			
PO	+ + +	+	+				
CM/PCN	+ + o o	+ + o	+ + +	+	+ +		
RM	+ +	+	+ +		+		
PPN	+		+ o			+	
CbCtx							
2						o o	
3	o o	o	o				
4/5	o o o	o o	o o o	o	o o	o o	
6	o o	o	o o			+ o o	
7				o		o	

8	o o		o	o		+ + o o o	
9			o	o o	o	+ + o o o o	
10				o		+ o	
Fl				o o		o o o	
PFl	o o	o		o		o o o	o
PM	o o o	o	o o	o	o o	+ o o	
Cop	o o o	o o	o o o	o o		+ o o	o
Cr1	o o	o	o	o	o o	o o	
Cr2	o o o	o o	o o	o	o o	+ o o	
Sim	o o o	o o	o o o	o	o o o	o o	

228

229 **Resources Table:**

230

Reagent type	Designation	Source	Identifiers	Additional information
Strain, strain background (*Mus musculus*)	C57BL/6J	Charles River	Stock	
Genetic reagent (*Mus musculus*)	Gad1-Cre	Gift from Dr. Diego Restreppo, recv'd frozen embryos from Tamamaki group		PMID: 19915725
Genetic reagent (*Mus musculus*)	Ntsr1-Cre	MutantMouse Regional Resource Center	Stock, Tg(Ntsr1-cre) GN220Gsat/ Mmucd	PMID: 17855595
Genetic reagent (*Mus musculus*)	Vgat-ires-cre knock-in (C57BL/6J)	Jackson Labs	Stock, #028862	PMID: 21745644
Recombinant DNA Reagent	AAV1.CAG.flex.GFP/ RFP	Addgene	51502 (GFP), 28306 (RF) Lot #: V41177 (GFP) Lot #: V5282 (RFP)	Titer: 2.0 x 10^{13} (GFP) 1.2X10^{13} (RFP)
Recombinant DNA Reagent	rAAV2.EF1a.DIO.eYFP.WPRE.pA	UNC	Lot #: AV4842F Addgene plasmid # 27056	Titer: 4.5X10^{12}
Recombinant DNA Reagent	AAV8.hysn-ConFon.eYFP	Addgene	55650 Lot #: V15284	PMID: 24908100 Titer: 2.97X10^{13}
Recombinant DNA Reagent	AAVretro-EF1a-FlpO	Addgene	55637 Lot # V56725	PMID: 24908100
Recombinant DNA Reagent	AAV2-retro-hSyn-cre (GFP-histone tag)	Viral preparations were a gift of Dr. Jason Aoto	Addgene plasmid number: 81070	
Recombinant DNA Reagent	AAV9- FLEX-H2B-GFP-2A-oG	Salk Institute	Cat #: 74829	PMID: 27149846 Titer: 2.41X10^{12}
Recombinant DNA Reagent	AAV1-EF1-FLEX-TVA-mCherry	UNC	Addgene plasmid#: 38044	PMID: 22681690
Modified Virus	EnvA-Gdeleted-EGFP	Salk Institute	Cat #: 32635	PMID: 17179932

				$3.47X10^7$

Supplementary Figures:

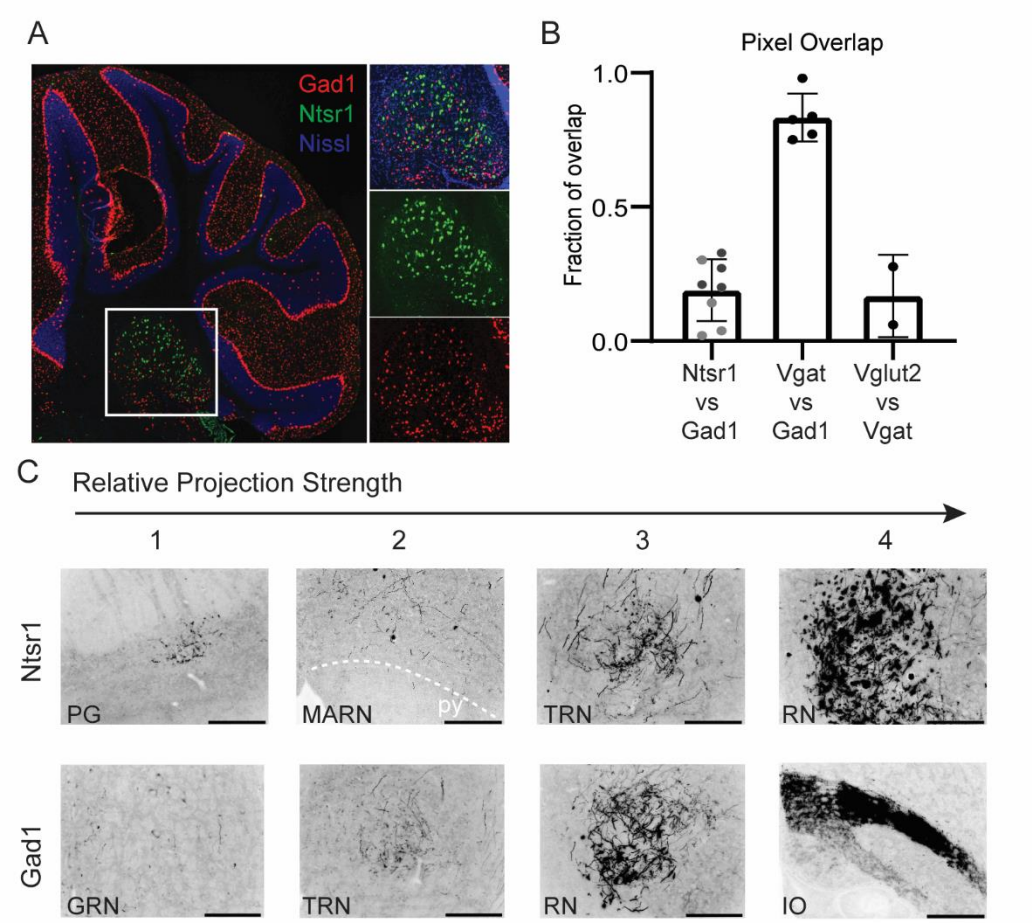

Supplemental Figure 1. Isolating cell populations and analyzing projection strength. (A) Dual fluorescent in situ hybridization showing nonoverlapping populations of Ntsr1+ and Gad1+ cells within IN. Insets show reporter overlap (top), Ntsr1 driven fluorescence (middle), and Gad1 in situ hybridization (bottom). (B) Quantification of fluorescent pixel overlap in Ntsr1-Gad1 (2 mice, 4 parasagittal sections each), Vgat-Gad1 (1 mouse, 5 parasagittal sections), and Vgat-Vglut2 (1 mouse, 2 parasagittal sections). Mean and standard error are plotted. (C) Example terminal fields in Ntsr1 or Gad1 specimens assigned relative projection strengths of 1-4. Note that anterior-posterior spread was also considered. Scale bar represents 200 µms.

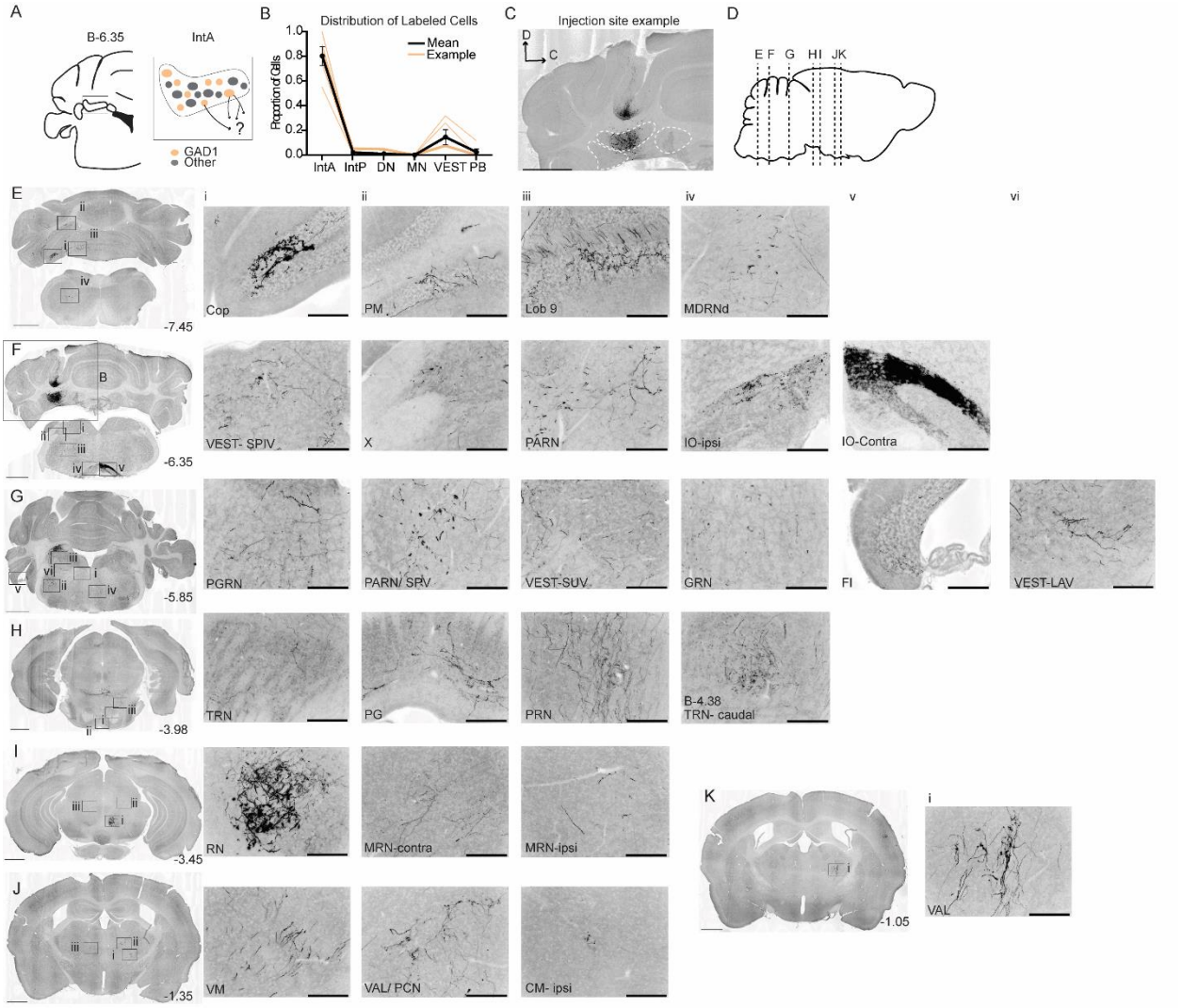

Supplemental Figure 2. Anterograde tracing of Gad1 projections from IntA (A) Ideal location for IntA injections (left) and depiction of Gad1+ cells within IntA (right). (B) Distribution of labeled cells by injection into IntA of Gad1-cre mice (left). All specimen in thin orange lines, example specimen shown to the right denoted by thick orange line, mean of all specimen plotted in black with SEM. (C) Example injection site of AAV2-Ef1a-DIO-EYFP in a Gad1-cre mouse (right). Images oriented so right of midline is contralateral. (D) Parasagittal mouse brain schematic showing location of coronal sections in E-K. (E) Projection targets in caudal cerebellum and brainstem (B-7.45). Boxes expanded in i-vi. (F) Projection targets within the intermediate cerebellum (B- 6.35). Injection site depicted in C. Note the dense projection to IO. (G) Projection targets within and ventral to the anterior cerebellum (B-5.85). (H) Projection targets to pontine nuclei (B-3.98 and B-4.38 (iv)). (I) Projection targets in the rostral midbrain (B-3.45). (J) Projection targets to the caudal thalamus (B-1.35). (K) Projection targets to the rostral thalamus (B-1.05). Scale bars (B, C, E-K) represent 1 mm and (i-vi) 200 µms.

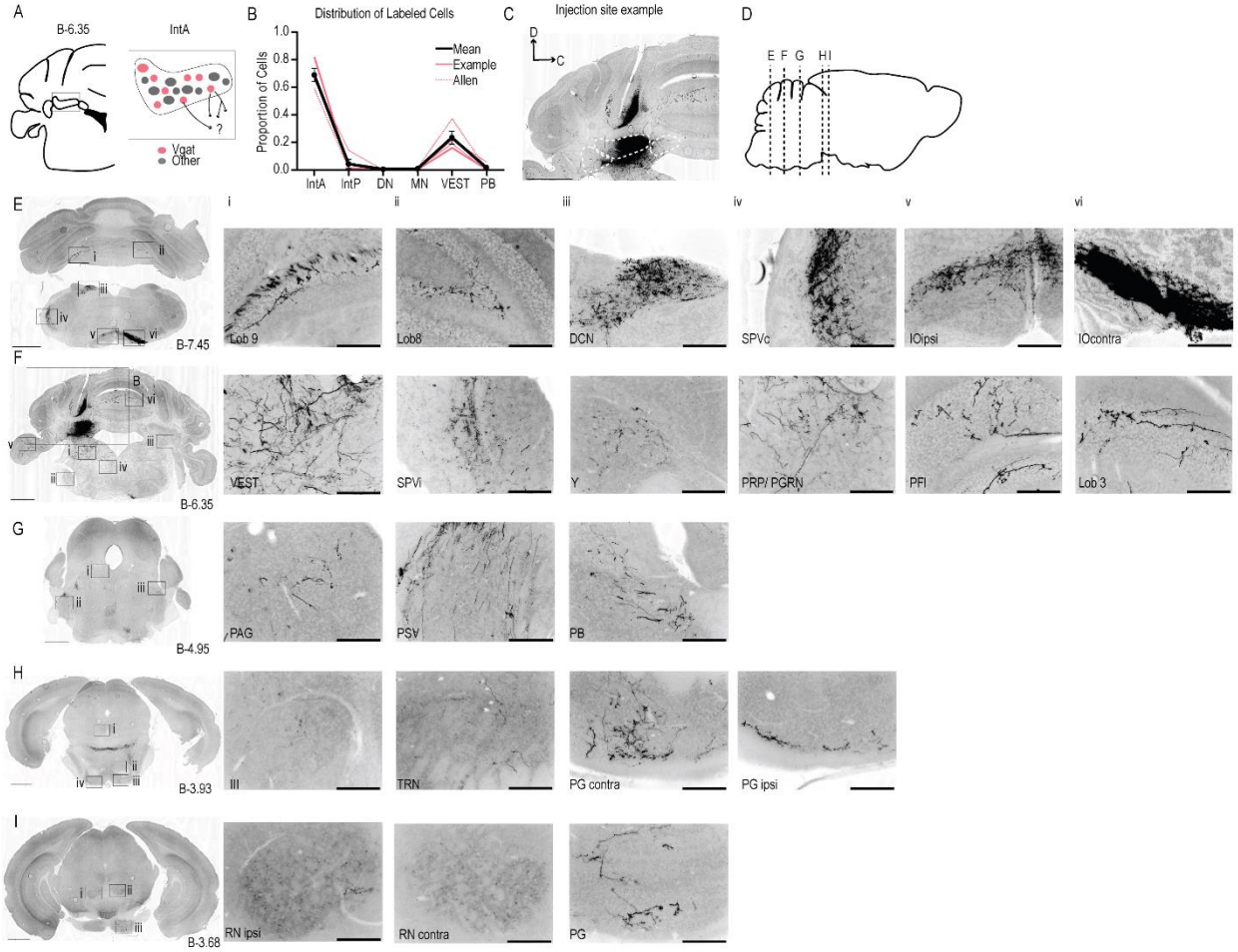

Supplemental Figure 3. Anterograde tracing of Vgat projections from IntA (A) Ideal location for IntA injections (left) and depiction of Vgat cells within IntA (right). (B) Distribution of labeled cells by injection into the CbN of Vgat-cre mice. All specimen in thin pink lines, example specimen shown to the right denoted by thick pink line, specimen gathered from the Allen denoted by dotted pink line, mean of all specimen plotted in black with SEM (C) Example injection site of AAV2-EF1a-DIO-eYFP. The three main CbN are outlined in white. Images oriented so right of midline is contralateral. (D) Parasagittal mouse brain schematic showing location of coronal sections in E-I. (E) Projection targets in caudal cerebellum and brainstem (B-.745). Boxes expanded in i-vi. (F) Projection targets within the intermediate cerebellum (B- 6.35). Injection site depicted in C. (G) Projection targets within rostral brainstem (B-4.95). (H) Projection targets in the caudal midbrain (B-3.93). (I) Projection targets to the rostral midbrain (B-3.93). Note sparse terminals in RN.

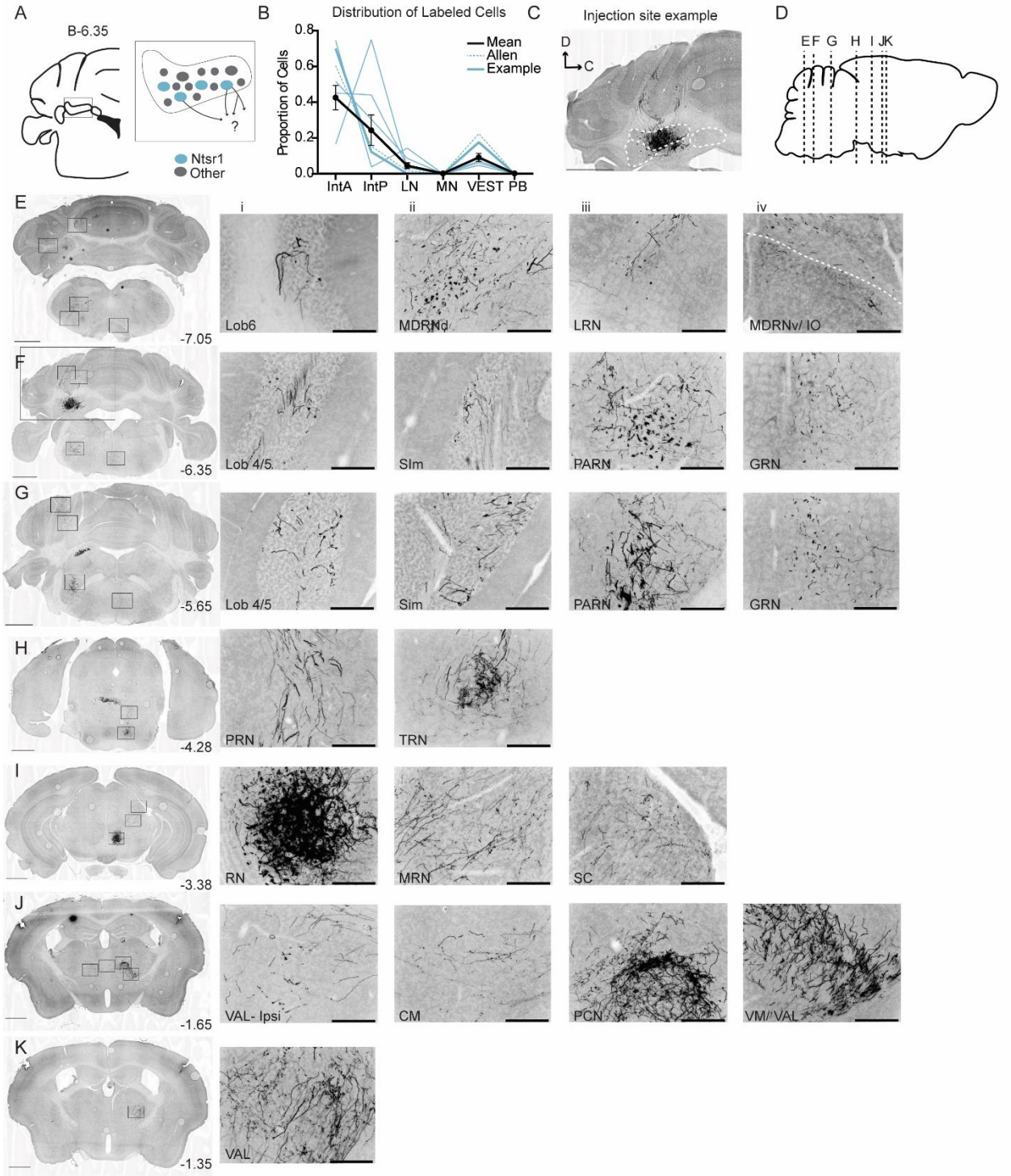

Supplemental Figure 4. Anterograde tracing of Ntsr1 projections from IntA. (A) Schematic of target. (B) Distribution of labeled cells by injection into the CbN of Ntsr1-cre mice. All specimen in thin blue lines, example specimen shown to the right denoted by thick blue line, specimen gathered from the Allen denoted by dotted blue line, mean of all specimen plotted in black with SEM (C) Example injection site of AAV2-EF1a-DIO-eYFP in an Ntsr1.cre mouse. The three main CbN are outlined in white. Images oriented so right of midline is contralateral. (D) Parasagittal mouse brain schematic showing location of coronal sections in E-K. (E) Projection targets in caudal cerebellum and brainstem (B-7.05). Boxes expanded in i-v. (F) Projection targets within the intermediate cerebellum (B- 6.35). Injection site depicted in C. (G) Projection targets within and ventral to the anterior cerebellum (B-5.65). (H) Projection targets to pontine nuclei (B-4.25). (I) Projection targets in the rostral midbrain (B-3.38). Note

the dense terminals in RN. (J) Projection targets to the caudal thalamus (B-1.65). (K) Projection targets to the rostral thalamus (B-1.35). Scale bars (B, C, E-K) represent 1 mm and (i-vi) 200 µms.

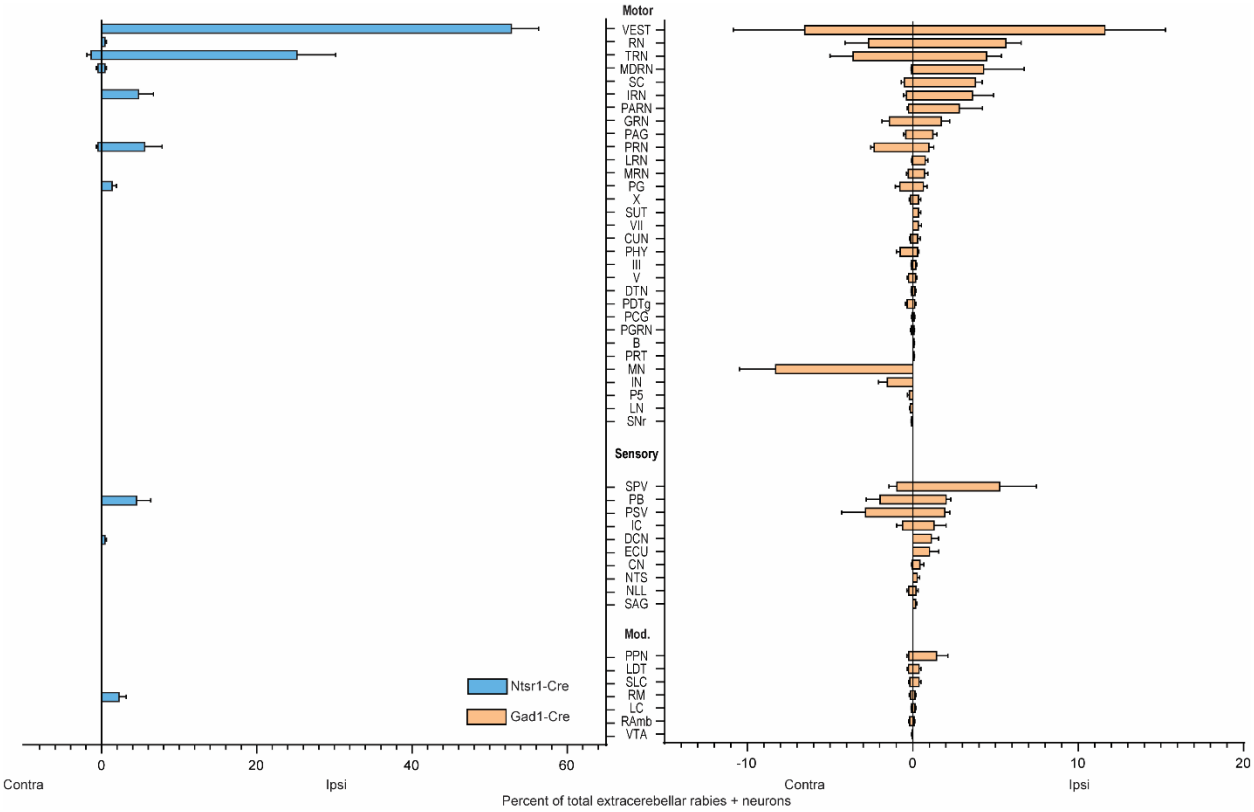

Supplemental Figure 5. Summary of monosynaptically labeled inputs to Gad1 (orange, n =3 mice) and Ntsr1 (blue, n =6 mice) neurons in IntA from extracerebellar regions. Mean and standard error are plotted.